Stutter: a Transient Dynamic Instability Phase that is Strongly Associated with Catastrophe

Shant M. Mahserejian[2,3,*,‡], Jared P. Scripture[1,*], Ava J. Mauro[1,10], Elizabeth J. Lawrence[5], Erin M. Jonasson[1,6], Kristopher S. Murray[1], Jun Li[2], Melissa Gardner[9], Mark Alber[2,4], Marija Zanic[5,7,8], and Holly V. Goodson[1,‡]

Author Affiliations:
[*]Co-first authors
[‡]Corresponding authors
[1]Department of Chemistry and Biochemistry, University of Notre Dame, IN 46566
[2]Department of Applied and Computational Mathematics and Statistics, University of Notre Dame, IN 46566
[3]Pacific Northwest National Laboratory, Richland, WA 99352
[4]Department of Mathematics, University of California Riverside, Riverside, CA 92521
[5]Department of Cell and Developmental Biology, Vanderbilt University, Nashville, TN 37240
[6]Department of Natural Sciences, Saint Martin's University, Lacey, WA 98503
[7]Department of Chemical and Biomolecular Engineering, Vanderbilt University, Nashville, TN 37235
[8]Department of Biochemistry, Vanderbilt University, Nashville, TN 37205
[9]Department of Genetics, Cell Biology, and Development, University of Minnesota, Minneapolis, MN 55455
[10]Department of Mathematics and Statistics, University of Massachusetts Amherst, Amherst MA, 01003

ABSTRACT

Microtubules (MTs) are dynamic polymers with critical roles in processes ranging from membrane transport to chromosome separation. Central to MT function is dynamic instability (DI), a behavior typically assumed to consist of growth and shortening, with sharp transitions in between. However, this two-state assumption disregards details in MT behavior that are evident in high-resolution data. For example, MTs exhibit growth rate variability, and pinpointing where transitions begin can be difficult when viewed at high spatiotemporal resolution. These observations suggest that MT behavior is more complicated than implied by standard quantification methods. To address these problems, we developed STADIA (Statistical Tool for Automated Dynamic Instability Analysis). STADIA's methods are rooted in machine learning to objectively analyze and quantify macro-level DI behaviors exhibited by MTs. Applying STADIA to MT length-history data revealed a transient, intermediate phase that we term 'stutter', during which the rate of MT length change is smaller in magnitude than growth or shortening phases. Significantly, most catastrophe events in both simulations and experiments are preceded by stutters, suggesting that this newly recognized phase is mechanistically involved in catastrophes. Consistent with this idea, a MT anti-catastrophe factor (CLASP2γ) increases the likelihood of growth following a stutter phase in experiments. We conclude that STADIA enables unbiased identification of DI phases including stutters, producing more complete and accurate DI measurements than possible with classical analysis methods. Identifying stutters as a distinct and quantifiable phase provides a new target for mechanistic studies regarding DI phase transitions and their regulation by MT binding proteins.

SIGNIFICANCE STATEMENT

Microtubules are cytoskeletal fibers that undergo dynamic instability, a remarkable process involving phases of growth and shortening separated by approximately random transitions (catastrophe and rescue). Dissecting the mechanism of dynamic instability requires first characterizing and quantifying these dynamics. We present a novel machine-learning based tool (STADIA), which shows that microtubule behavior consists not only of growth and shortening, but also a transient intermediate phase we term "stutter." Quantifying stutter and other dynamic behaviors with STADIA shows that most catastrophes in simulations and experiments are preceded by stutters, and that the anti-catastrophe factor CLASP2γ works by increasing the fraction of stutters that revert to growth. STADIA provides new opportunities for analyzing mechanisms of microtubule dynamics and regulation by binding proteins.

INTRODUCTION

Microtubules (MTs) are protein-based biological polymers that have a central role in fundamental eukaryotic processes including cellular organization, chromosome separation during cell division, and intracellular transport (Goodson and Jonasson 2018). Crucial to the function of MTs in these processes is a well-known behavior termed dynamic instability (DI), where the polymers switch stochastically between periods of growth and shortening (Mitchison and Kirschner 1984; Desai and Mitchison 1997). Accurate quantification of DI provides a needed foundation for understanding the significance of this behavior *in vivo* and for investigating the activities of MT regulating proteins *in vitro*.

Problems with current methods of quantifying DI metrics

Traditionally, MTs have been treated as two-state polymers; that is, MTs have been considered to be either growing or shortening, with abrupt, instantaneous transitions called catastrophes and rescues between these two phases (**Figure 1 A,B,D**). In this framework, MT behavior is characterized by four quantities called DI parameters: F_{cat} (frequency of catastrophe, measured as the number of catastrophes per time in growth), F_{res} (frequency of rescue, measured as the number of rescues per time in shortening), V_{growth} (velocity of growth, measured as the mean of the growth rates over the set of growth phases), and V_{short} (velocity of shortening, measured as the mean of the shrinkage rates over the set of depolymerization phases) (Walker et al. 1988). While determination of DI parameters is now the standard way to quantify MT behavior, there are several issues with using this approach.

First, it has long been recognized that both growth and shortening rates are variable throughout a given phase segment and between different segments; this variability occurs both with and without MT binding proteins (MTBPs) (see e.g., (Pedigo and Williams 2002; Elizabeth J. Lawrence et al. 2018; Gildersleeve et al. 1992)). This observation raises the concern that averaging across an entire growth or depolymerization phase could cause finer but functionally significant aspects of MT behavior to be missed and potentially result in problems with precision and reproducibility.

Second, recent improvements in imaging technology have enabled acquisition of MT growth data with both high temporal and spatial resolution. These data have verified the intrinsic variability of MT behavior, and they have also demonstrated that there can be significant time periods (e.g., a few seconds in duration) during which MTs do not change appreciably in length (**Figure 1 C,E;** see also (Maurer et al. 2014; Duellberg, Cade, and Surrey 2016; Rickman et al. 2017; Duellberg et al. 2016)). These relatively flat sections of length-history plots cannot be unambiguously categorized as either growth or shortening, and thus the limitations of the two-state behavior assumption become apparent. Because including these slow-down periods in either growth or depolymerization phases would reduce measured values of V_{growth} and V_{short}, they have sometimes been excluded from quantification of DI parameters (e.g., (Rickman et al. 2017)). However, entirely excluding these behaviors from analysis could potentially result in the loss of information critical for understanding the mechanisms of the phase transitions or their regulation by MT binding proteins. Thus, capturing and quantifying these alternative behaviors is a key step towards explaining the recognized variations in growth and shortening rates, improving the precision of these metrics, and elucidating mechanisms of dynamic instability.

The advent of high-resolution data acquisition has revealed an additional problem with standard DI analysis: it can be difficult to determine with reasonable precision where transitions between phases begin and end (**Figure 1 C,E**). This observation leaves researchers to make subjective judgments or to use 'in-house' software with non-adaptive criteria to identify the points where phase transitions occur (e.g., (Yenjerla, Lopus, and Wilson 2010; Goodson and Jonasson 2018; Zanic 2016)). To illustrate this problem, consider the zoomed-out length-history plots that are typically used for DI analysis (**Figure 1 B,D**). Examination of these plots can make the task of determining when transitions occur look trivial. However, the zoomed-in views made possible by high-resolution data acquisition demonstrate that any software or method using the aforementioned two-state behavior framework will have difficulty categorizing ambiguous behavior that often occurs between growth and shortening phases (**Figure 1 C,E**).

Taken together, these issues indicate that there is significant need for an improved method of characterizing MT length-history data that removes the two-state behavior assumption and allows for unbiased, objective quantification of MT behavior and DI metrics.

Summary of results

Using established machine learning and statistical methods, we developed the Statistical Tool for Automated Dynamic Instability Analysis (STADIA), an automated and unbiased tool for characterizing and quantifying MT behavior. Applying STADIA to *in silico* and *in vitro* MT length-history data revealed the existence of 'stutter,' a previously uncharacterized, transient DI phase where MTs exhibit rapid low-amplitude fluctuations but with an overall rate of change in MT length that is markedly less in magnitude compared to growth and shortening phases. Significantly, we observed that most catastrophes, 78% *in silico* and 86% *in vitro*, are preceded by stutters, and that the MT stabilizing protein CLASP2γ reduces catastrophe by increasing the fraction of stutters that return to growth rather than enter shortening phases. These results indicate that classical methods of analyzing MT behavior miss mechanistically significant aspects of MT behavior and that our novel DI analysis tool, STADIA, is able to recognize and quantify these behaviors. We conclude that identification of stutters as a phase distinct from growth and shortening warrants their future inclusion in DI analyses, and serves as a necessary step forward in gaining a better understanding of MTs, their dynamics, and their regulation by MT binding proteins.

RESULTS & DISCUSSION

We first present a brief overview of STADIA and its analysis procedure (readers are encouraged to refer to the Methods for more detailed information). We then use STADIA to analyze MT dynamics as they are observed in simulations (*in silico*) and in experiments (*in vitro*); this work leads us to identify the existence of a transient, intermediate phase that we term 'stutter'. We use this observation as a foundation on which to study the relationship between stutter and the phase transitions, showing that stutter is strongly associated with catastrophe. We further test the functional significance of this observation and demonstrate the utility of STADIA in studying MT-binding proteins by using STADIA to

analyze the dynamics of MTs growing in the presence of the anti-catastrophe factor CLASP2γ, thus examining for the first time its effect on stutter.

STADIA: A Novel Tool for Analyzing Dynamic Instability Behavior of MTs

To meet the goal of more precisely identifying, categorizing, and quantifying the range of MT behaviors, we created the Statistical Tool for Automated Dynamic Instability Analysis (STADIA). Specific aims for the development of STADIA were that it be: **1)** Automated to create a consistent and reproducible method with minimal user input; **2)** Unbiased to remove any assumptions about MT dynamics being restricted to two states (i.e., being limited to growth and shortening); **3)** Adaptive to handle varying time durations and the stochastic nature of phase changes; **4)** Compatible with classical DI analysis, enabling comparison to and continuity with previous work; **5)** Capable of analyzing data sourced from both computational simulations and laboratory experiments.

The resulting software, STADIA, is a data-driven tool that uses machine learning to characterize and quantify MT behavior. The process, implemented in MATLAB, has three major stages (**SuppMat Figure S1**):

1) Segmentation: STADIA creates a continuous piecewise linear approximation of MT length-history data, where segment endpoints mark moments of significant change, i.e., transitions between periods of sustained behavior (**Figure 2**).
2) Classification: STADIA then classifies the individual segments from the linear approximation using an unsupervised clustering method, *k*-means, and bundles clusters with similar characteristics into phases (**Figure 3, SuppMat Figures S2,S3,S4,S5**).
3) Phase and Transition Analysis: STADIA then applies the segment classifications to length-history plots and characterizes each phase and transition quantitatively (**Figure 3 G,H, Table 1, SuppMat Figure S9**).

STADIA can be run in automated mode (outlined above; used for performing full DI analysis) or diagnostic mode (useful for performing preliminary analyses and tuning analysis parameters, mentioned below). More information about the process by which STADIA analyzes and quantifies dynamic instability is provided in the Methods and Supplementary Information.

In initial testing, we used STADIA to analyze data from our detailed kinetic Monte Carlo model of MT dynamics (model described in Methods section) under settings where we forced STADIA to assume that MT dynamics consist only of growth and shortening phases. As expected, under these constrained conditions, the DI parameters measured by STADIA were consistent with those measured through traditional DI analysis; similar results were obtained when STADIA was used to analyze data from *in vitro* dynamic instability experiments under the same constraints (**Table 1**). These observations provided a solid foundation on which to proceed with using STADIA to analyze DI without preconceptions about how many distinguishable phases exist in MT length-history data.

Gap statistic analysis provides evidence for multiple types of growth and depolymerization behavior in both simulation and experimental data

As mentioned above and described more in the Methods and Supplementary Information, STADIA clusters individual MT length-history segments into groups (which may or may not correspond to recognizable DI phases). Clustering is performed using an unsupervised clustering method, which means that the method does not presuppose that the clusters correspond to any particular DI phase; after the segments are assigned to clusters, the DI phase to which each cluster belongs will be determined based on cluster metrics. The particular method we use is called *k*-means clustering, and requires that the desired number of clusters, *k*, is provided in advance (see the Methods for more information regarding *k*-means clustering and its use in this analysis). Though various approaches exist for determining the *k*-value with which to perform the clustering (reviewed by (Steinley 2006; Pham, Dimov, and Nguyen 2005)), STADIA uses a measurement called the gap statistic (Tibshirani, Walther, and Hastie 2001). Briefly, with STADIA running in diagnostic mode, the value of the gap statistic at each integer *k* is evaluated for a dataset and compared to results at other *k* values to indicate how well a dataset can be described by *k*-many clusters. Generally, the value of *k* at which the gap statistic plot attains its first local maximum is considered to be the optimal number of clusters, though decisions about what *k*-value is most appropriate should consider other aspects of the data as well (Tibshirani, Walther, and Hastie 2001). The scientist using STADIA is meant to take the suggestions from the diagnostic mode and supply appropriate *k*-values to obtain final clustering results from the automated mode.

Initial Observations

Using the two datasets (*in silico* and *in vitro*) already analyzed in Table 1, we performed analysis using the gap statistic to determine which of the following two possibilities is better supported: (1) that MT dynamics adhere to two-state behavior, consisting of only growth and shortening, with instantaneous transitions between these two states; or (2) that MT behavior is more complex, consisting of additional behaviors and transitions. Applying the gap statistic calculation to the entire dataset (either *in silico* or *in vitro*), such that all types of segments (positive and negative slopes) were considered together, did not identify an optimal number of clusters (**SuppMat Figure S6**). We moved forward by treating positive and negative slope segments separately to determine if each consists of either one or multiple clusters.

Separate analysis of growing and shortening segments

We calculated the gap statistic separately for the positive and negative slope segments, after removing the set of segments with approximately zero-slope (since flat segments obviously do not belong to either growth or shortening phases and should thus be treated separately). Performing analysis with the gap statistic in this manner on the *in silico* data suggested *k*=3 to be the optimal number of clusters for both the positive and negative sloped segment groups (**Figure 3 A,D & SuppMat Figures S4,S5**). These observations indicate that the *in silico* dataset contained multiple clusters of growth and shortening behaviors. In total, when including the near zero-slope segments, 7 distinct clusters were identified in simulation data (**SuppMat Figure S7**).

Consistent with the *in silico* results, the analysis of the *in vitro* experimental data suggested *k*=3 for positive slopes (**Figure 3 B** and **SuppMat Figure S4**). However, differences were found between the *in*

silico and *in vitro* data in analysis of the negative slopes: the optimal number of clusters was identified to be two (*k*=2) in both experimental datasets (**Figure 3 E** and **SuppMat Figure S5**), in contrast to the three clusters identified in the simulation data. This observation can be explained by the fact that for technical reasons, the *in vitro* dataset contains the beginning of shortening phases, but not the full loss of MTs to near-zero length, which was available with the simulation data. Consistent with this explanation, inspection of the clustering results for the negative slope segments in **Figure 3** shows that segments belonging to Negative Slope Cluster 3 (the cluster with the longest time durations) in the *in silico* data in **Figure 3 D** were not captured for the *in vitro* data in **Figure 3 E**. Therefore, we can only conclude that there are *at least* two clusters with negative slopes for the *in vitro* data. For illustration purposes, a "ghost" region is added to **Figure 3 E** where we expect the missing third negative slope cluster to reside. Thus, including the flat slope segments, we find evidence for at least 6 distinct clusters in the experimental DI data: three clusters of growth, two clusters of shortening, plus the small number of flat slope segments used to separate the positive and negative slope segments (**SuppMat Figure S7**). An additional cluster of shortening segments might be identified if full depolymerization events were captured in experiments.

In summary, application of gap statistic analysis to DI data from either simulations or experiments leads to a similar conclusion: the data argue against the idea that MT DI can be characterized as a two-state process consisting only of growth and shortening with instantaneous transitions. More specifically, the results provide evidence for considering multiple types of growth behavior (3 clusters) and multiple types of shortening behavior (3 clusters, or 2 clusters for the truncated experimental data). In the next section, we examine the differences between these clusters of length-history segments to determine how the segments in these clusters differ from each other and how these clusters might correspond to recognizably different phases of DI behavior.

STADIA can identify growth and shortening phases consistent with those identified by classical DI analysis

After using STADIA in diagnostic mode to perform gap statistic analysis and thus gain information about the optimal number of clusters to use in the *k*-means clustering process, we used STADIA in the automated mode to perform a full analysis of MT behavior. In the automated mode, STADIA first determines the centroid of each cluster of length-history segments. It then categorizes each segment identified from the segmentation stage as belonging to one cluster or another (see **SuppMat Figure S1** for an outline of the full analysis process; see the Methods section for more details). To study the relationships between these clusters of length-history segments and recognizable phases of DI, we examined the average characteristics of the segments in each group.

This analysis showed that, for both the *in silico* and *in vitro* data, some of the clusters correspond to the well-recognized growth and shortening phases of DI. More specifically, two of the positive segment clusters (positive slope clusters 1 and 2 from **Figure 3 A and B)** have slopes (rates of length change) similar to growth rates reported in classical DI analysis (compare STADIA results in **Figure 3 C** and **Table 1** to classical analysis results in **Table 1**). Similarly, negative slope cluster 2 (*in silico* and *in vitro*, **Figure 3 D and E**) and negative slope cluster 3 (*in silico*, **Figure 3 D**) have slopes similar to shortening rates

reported in classical DI analysis (compare **Figure 3 F** and **Table 1**). Based on this information, in the classification stage of STADIA, length-history segments were assigned to the growth phase if they belonged to one of the clusters with a steep positive slope (Positive Slope Cluster 1 or 2 in **Figure 3 C,I**), and to the shortening phase if they belonged to a cluster with a steep negative slope (Negative Slope Cluster 2 or 3 in **Figure 3 F,I**).

The identification of two clusters within the bundled growth phase (and for the *in silico* data, within the bundled shortening phase) is unexpected. It is notable that in each case (both positive and negative slopes), the clusters differ primarily by duration (brief or sustained, **Figure 3I** and **SuppMat Figure S8**). This observation may be evidence of different behaviors of tapered or split tips (e.g., as observed by (Coombes et al. 2013; Doodhi et al. 2016; Aher et al. 2018)) relative to the rest of the MT; such structures might be able to extend or retract faster than the bulk MT lattice in the absence of lateral bonds. Future work will investigate whether the differences between brief and sustained growth (or shortening) relate to tip structure.

In the next section, we consider the length-history segments that have much shallower slopes, which set them apart from the other growth and shortening behaviors discussed above.

'Stutters': a distinct phase identified in MT DI behavior

Examination of **Figure 3 A-F** shows that, in addition to clusters with slopes that correspond to rates of length change seen in classical growth or shortening behaviors, STADIA also identifies clusters with much shallower slopes (Positive Slope Cluster 3 and Negative Slope Cluster 1 in **Figure 3 A-F; Table 1**). Moreover, the segments in these shallow-slope clusters have time durations much shorter than typical segments classified as sustained growth and sustained shortening, though typically longer than those recognized as brief growth and brief shortening segments (**SuppMat Figure S8**). We term these shallow-slope clusters of segments 'stutters' to convey the idea that these sections of length-history data exhibit high-frequency, low-amplitude fluctuations throughout which the MT length changes little from a macro-level perspective.

Note that stutters are distinguishable from previously identified 'pauses', which are periods longer in duration (typically > 15 seconds), during which the MT neither grows nor shortens detectably (Yenjerla, Lopus, and Wilson 2010). In contrast, MT lengths do indeed change dynamically during stutter periods, though the net rate of change is small. In addition, it is notable that events categorized as pauses are typically described as being rare (<1% of total behavior duration) in the absence of MT stabilizing proteins (e.g., (Walker et al. 1988; Moriwaki and Goshima 2016)). These observations support the conclusion that stutters are different from events previously classified as pauses, though there is likely some overlap, especially in cases where events categorized as pauses are allowed to be short in duration (e.g., (Walker et al. 1988; Guo et al. 2018)). Stutters as described above likely encompass the periods of slowed growth or shortening previously noted (but not quantified or characterized) in recent dynamic instability data acquired at high spatiotemporal resolution (e.g,. (Rickman et al. 2017; Duellberg, Cade, and Surrey 2016); see also (Margolin et al. 2012)). In contrast to previous work, we quantify and consider the role of stutters in DI as part of the procedures included in STADIA.

Together, these characteristics indicate that these transient periods of little length change are clearly distinct from either classical growth or shortening phases. Thus, we assigned these clusters with shallow slopes to a new DI phase class, 'stutters'. The stutter phase consists of 'up stutters' (Positive Slope Cluster 3), 'flat stutters' (Near-zero Slope Cluster) and 'down stutters' (Negative Slope Cluster 1) depending on whether the shallow slopes are positive, near zero, or negative, respectively (**Figure 3 I**).

At this point, every segment of length-history has been classified, and the assignment of individual segments to growth, shortening, and stutter phases can be visualized in the context of the original length-history data as in **Figure 3 G,H**.

MTs spend a significant fraction of time in the stutter phase

We begin to investigate the significance of stutter by first examining the fraction of time that MTs spend in the stutter phase. As one might expect, both *in silico* MTs and physical MTs spend the majority of their time in growth phases. However, in both simulations and experiments, MTs spend a substantial amount of time in stutter phases. Notably, in our *in silico* datasets, the MTs spent more time in stutter (8%) than in shortening (6%) (**Figure 4 A; SuppMat Figures S8,S9**). For *in vitro* MTs, a substantial amount of the time for the observed MTs was spent in the stutter phase (**SuppMat Figures S8,S9**), but direct comparison to time spent in the shortening phase is not conclusive because depolymerizations were not fully captured. Given other similarities between the simulated and physical MTs, it seems likely the ratio of time in stutter to time in depolymerization would be similar to that observed with simulation MTs. These observations indicate that stutters contribute appreciably to MT behavior as assessed in length-history plots.

Catastrophes are usually preceded by stutters *in silico* and *in vitro*

To investigate the functional significance of stutters, we used STADIA to examine how transitions between phases occur (**Figure 4 B-I; Figure 5**). Specifically, we wished to quantify all examples of transitions between growth, shortening, and stutter (in any order). Considering the chronological ordering of phases, STADIA automatically categorized catastrophes and rescues as being either 'abrupt' (if the switch between growth and shortening occurred without a detected stutter between them) (**Figure 4 D,E; Figure 5 D,E**) or 'transitional' (if a stutter phase occurred during [at] the switch between growth and shortening phases) (**Figure 4 F,G; Figure 5 F,G)**. We also identified 'interrupted growth' (when a stutter occurred between two periods of growth) (**Figure 4 H; Figure 5 H,I**) and 'interrupted shortening' (when a stutter occurred between two periods of shortening) (**Figure 4 I**).

Remarkably, when we examined the simulation data, we found that 78% of catastrophes commenced with a stutter, i.e., were transitional (**Figure 4 B**). A related observation is that almost half (44%) of stutters that occurred during growth ended in catastrophe (**Figure 4 C**). A similar but more dramatic association between stutter and catastrophe was observed *in vitro*: 86% of catastrophes commenced from a stutter (**Figure 5 A**), and 75% of stutters during growth ended in a catastrophe (**Figure 5 B**).

In contrast to catastrophes, rescues as observed *in silico* rarely occurred with stutter. More specifically, only 5% of *in silico* rescues were transitional (i.e., few rescues initiated from a stutter phase) (**Figure 4 B**), and only 8% of stutters that occurred during depolymerization resulted in a rescue (**Figure 4 C**). Because we do not have data for rescues *in vitro*, we cannot make strong conclusions on the correlation between stutters and rescue in physical MTs. However, these results do suggest that catastrophe and rescue are not simply the mechanistic opposites of each other.

CLASP2γ reduces the frequency of catastrophe by increasing the prevalence of interrupted growth

To further test STADIA's utility in analyzing dynamic instability and examine both the prevalence and significance of stutters, we analyzed another, comparable *in vitro* dataset in which the MTs were polymerizing in the presence of the MT binding protein CLASP2γ, which has been previously characterized as an anti-catastrophe factor (E. J. Lawrence and Zanic 2019; Aher et al. 2018). Qualitatively, the results obtained from using STADIA to analyze length-history data generated in the presence of CLASP2γ were similar to those with the control MTs *in vitro*. Most significantly, separable stutter phases were again observed (**SuppMat Figure S4,S5**).

However, dramatic differences between the CLASP2γ data and control *in vitro* data were observed when these data were examined quantitatively. First, the frequency of transitional catastrophes in the presence of CLASP2γ was significantly reduced (**Figure 5 A** and **SuppMat Figure S10**). This itself is not surprising, given that previous work (e.g., (Elizabeth J. Lawrence et al. 2018; Sousa et al. 2007; Aher et al. 2018; Majumdar et al. 2018)) has shown that CLASP2γ reduces the frequency of catastrophe (see also **Figure 5 C**). Strikingly, however, CLASP2γ also increased the frequency of interrupted growths (growth-stutter-growth) (**Figure 5 B** and **SuppMat Figure S10**). More specifically, among transitions that begin as growth-to-stutter, CLASP2γ increased the proportion that are growth-stutter-growth and decreased the proportion that are growth-stutter-shortening **(Figure 5 B).** Taken together, these data demonstrate that STADIA analysis provides information about CLASP2γ function not supplied by traditional analysis and indicates that CLASP2γ suppresses catastrophe at least in part by enabling stuttering MTs to re-enter the growth phase. This idea is supported by recent reports that MTs can withstand greater growth rate variability without undergoing catastrophe in the presence of CLASP2γ (Elizabeth J. Lawrence et al. 2018; E. J. Lawrence and Zanic 2019) and that CLASP2γ can protect against catastrophe in the presence of lagging protofilaments (Aher et al. 2018).

Mechanisms of stutters and implications for the process of catastrophe

What causes stutters, especially those that disrupt growth, and why are they associated with catastrophe? An important clue comes from recognizing that when transitioning from growth to stutter, there is a net decrease in the number of subunits that are incorporated into the MT per unit time. This net decrease could occur because new subunits attach to the tip less frequently than during normal growth, or because bound subunits leave the tip more frequently than during growth, or a combination of these two.

While simple stochastic fluctuations in subunit arrival or departure could potentially contribute to stutters, changes in rates of attachment and detachment could also result from changes in tip structure.

However, one could argue that the rate of subunit attachment should not vary with tip structure: assuming that longitudinal bonds form first, there are always 13 landing sites for new subunits (Castle and Odde 2013). Therefore, we suggest that stutters following growth segments likely result from a situation where an unusually large fraction of incoming subunits detach from the tip structure without being fully incorporated into the lattice, e.g., because tip taper or other structural features make it difficult for lateral bonds to form. In other words, we suggest that stutters occur when the structure of the tip is such that the subunit detachment rate is unusually high compared to the average detachment rate during growth. This reasoning provides a potential explanation for the correlation between stutter and catastrophe: if fewer subunits are incorporated into the lattice than normal, the stabilizing cap of GTP-tubulin at the MT end will become smaller, the likelihood of exposing GDP-tubulin subunits will increase, and the possibility of complete cap loss (catastrophe) will rise. At present, these ideas are speculation, but future work may be able to shed light on these hypotheses.

CONCLUSIONS

The key results of this work are four-fold: (1) the development of STADIA as an improved analytical tool for quantification of MT behavior; (2) the use of STADIA to identify 'stutter', a previously uncharacterized and unquantified phase in MT dynamics; (3) the observation that stutter is strongly associated with catastrophe *in silico* and *in vitro*; (4) the evidence that the anti-catastrophe factor CLASP2γ reduces catastrophe by increasing the fraction of stutters that return to growth rather than enter shortening phases. We suggest that quantification of stutters in future DI analysis through STADIA or similar tools will enable improved analysis of MT dynamics that is more complete, precise and reproducible. The clearer picture that results from this analysis will facilitate investigation of the mechanisms of catastrophe and rescue and the activities of the MT binding proteins that regulate these transitions.

METHODS

CLASSICAL DI ANALYSIS

In the classical DI analysis, growth and shortening phases were identified as described in the Supplemental Methods of (Jonasson et al. 2019). Briefly, using a custom MATLAB script [program], major peaks in the length-history data were identified, and then the ascent to each major peak was classified as a growth segment and the descent from the peak was classified as a shortening segment. For the analysis in this paper, the minimum prominence for major peaks (minimum height change between a major peak and the nearest major valley) in the classical DI analysis was set equal to the maximum height error tolerance in STADIA. The minimum peak height and the minimum rescue length in the classical DI analysis were set equal to the sum of the nucleation height threshold plus the maximum height error tolerance in STADIA (see **SuppMat Table S1**).

V_{growth} and V_{short} were calculated as follows. A linear regression was fitted to each growth or shortening segment. V_{growth} was calculated as the arithmetic mean of the slopes of the regression lines for all growth segments whose linear regression had an R^2 value of at least 95%. V_{short} was calculated in the same manner using the shortening segments. F_{cat} was calculated as the total number of catastrophes

divided by the total time spent in growth phases. Similarly, the F_{res} was calculated as the total number of rescues divided by the total time spent in shortening phases.

STATISTICAL TOOL FOR AUTOMATED DYNAMIC INSTABILITY ANALYSIS: STADIA

This section outlines the three major stages of STADIA analysis (Segmentation, Classification, and Phase and Transition Analysis) as well as the parameters used for the inspection of *in silico* and *in vitro* data using STADIA. Refer to **SuppMat Table S1** for a complete list of all STADIA user-defined parameters used for analysis of both *in silico* and *in vitro* MTs.

Segmentation

In the segmentation stage, STADIA takes MT length-history data and generates a continuous piecewise linear approximation of the MT length-history plot. Segmentation also includes a preprocessing step that prepares the user's length-history data for input into STADIA and a post-processing step that prepares the results of the segmentation step for classification.

Preprocessing: As an initial step, STADIA automatically formats the inputted MT length-history data into a single time series of length-history data points. MT length-history data can be provided either as a long-time observation of a single MT (possible with simulations) or as a series of length histories of multiple MTs (common with experimental data). In the latter case, STADIA automatically connects, or 'stitches', the data from multiple MTs (with separators in between) into a single time series representation of MT length-history data. Note that special treatment of the stitching separator between observations allows the segmentation to avoid misclassification of stitch boundaries as transitions. This preprocessing step allows STADIA to conduct analysis for both simulation data and experimental data in a similar and consistent manner.

In this manuscript, the simulation data were provided as one long time series from an individual MT (no stitching required), while the *in vitro* data (both with and without CLASP2γ) were obtained from multiple MTs over a shorter period of observation (for details, see *Data Acquisition – In Vitro Microtubule Experiments* in the Supplemental Material). Because long depolymerization phases were not captured (for technical reasons), the data from a specific MT were broken into samples that typically consisted of a growth phase followed by an initial depolymerization and then termination of that observation. STADIA first placed individual length-history samples for a given MT consecutively into the same time series plot, and then stitched all of the data for all of the MTs within each experiment. Note that the clustering methods used in STADIA require a dataset large enough to display a rich variety of possible DI behaviors. Therefore, instead of analyzing each individual *in vitro* MT for various behaviors, it is necessary to collectively consider multiple MTs from the same experiment so there is enough length-history data to classify. Thus, this stitching procedure captured all the available behavior from the *in vitro* experimental conditions into single time series representations (one with CLASP2γ and one without).

Segmentation: STADIA takes the single time series graph produced by the preprocessing step and performs segmentation as an adaptive, iterative process according to restrictions provided by user-

defined thresholds. The segmentation process begins by identifying major peaks and valleys (i.e., local extrema) in MT length-history data using the *findpeaks()* function in MATLAB. Consecutive extrema are connected by line segments to form an initial linear approximation of the length-history data (**Figure 2 C**). These peaks and valleys serve as the initial list of vertices used to construct the continuous piecewise linear approximation. The iterative process seeks to include new vertices to define line segments to improve accuracy (**Figure 2 D**) as follows: For each segment between two vertices, the error is calculated between each point in the length-history data and its corresponding approximation on the line segment. If the maximum error from this segment is less than the user-defined tolerance, then the error condition is satisfied, and the process moves onto the next segment. If the maximum error is greater than the user-defined tolerance, then the data point where the greatest error occurs is identified as a new vertex and an additional line segment is added (i.e., 1 segment is broken into 2 at the point with greatest error). This process effectively resolves the approximation error at that point by capturing a point where significant and sustained change in MT behavior occurs, thus improving the accuracy. When selecting new vertices, the algorithm is careful not to violate the user-defined minimum duration constraint, which ensures a macro-level approximation is constructed by limiting how close two vertices can be to each other.

This process is repeated until all line segments in the approximation meet the error tolerance requirement while also meeting the minimum time-step constraint. The result is a continuous, piecewise linear approximation that fits the whole of the length-history dataset according to a user-defined error threshold (excerpts of the full length-history approximation are illustrated in **Figure 2 D**, and the black lines plotted in **Figure 3 G,H**). The vertices of the piecewise linear approximations provide line segments with endpoints at exact moments where significant and sustained changes in MT behavior occur. Thus, the activity covered by each segment between endpoints represents a consistent period of MT length-history behavior that can be identified as belonging to a DI phase in the classification stage.

The following user-defined parameters set the accuracy of the piecewise linear approximations for all datasets considered in this study: Minimum Duration = 0.5 seconds; Error tolerance threshold = 20 subunits.

Post-processing to prepare for classification: Line segments from the piecewise linear approximation each have measured slopes, time durations, and height changes (**Figure 2 E**); this set of measurements provides a 3-D feature space where the segments reside. However, some post-processing is needed before submitting this dataset to the classification process. First, new vertices are added to mark the boundaries between which the MT lengths are below a threshold length, generally chosen to be near the limits of observation in experimental conditions. These periods of time are described as 'nucleation' and are excluded from other analysis. Next, line segments are identified as flat stutters if either their total height change or slope magnitude are below user-defined thresholds. Flat stutters are set aside until the end of the classification procedures. The remaining positive and negative sloped segments are considered separately during the next stage (classification).

In this work, line segments containing MT lengths less than 75 subunits were considered nucleation segments. Segments were identified as flat stutters if the total height change was less than 3 subunits or the absolute value of their slopes was less than 0.5 subunits/second.

Classification

In the classification stage, STADIA takes the results of the segmentation stage (segregated positive and negative sloped line segments that approximate the MT length-history data) and analyzes them using *k*-means clustering in conjunction with the gap statistic.

Justification for using k-means clustering: As noted at the beginning of the Results and Discussion section, one criterion for developing STADIA was that it be unbiased as to the number of behaviors exhibited by MTs to remove any assumptions about MT dynamics being restricted to two behaviors (i.e., only growth and shortening). The need for an unbiased classification process mandates the use of an unsupervised machine learning method, of which selection is limited. Because of its ability to identify locally dense substructures within data of various types, we chose to use *k*-means to handle classification of MT length-history data. Ideal datasets for *k*-means follow a Gaussian distribution and are regularly (globularly) shaped. Although our data is not Gaussian, *k*-means still provides an objective methodology to find substructures in the overall data structure. The observation that *k*-means enables us to identify and quantify stutters (a behavior that has previously been noted but not quantified) indicates that it provides a useful methodology for unbiased categorization and quantification of MT behavior.

Preprocessing: *K*-means clustering uses Euclidean distance (i.e., straight-line distance between two points in 3-D space) as the primary measurement in its algorithm to classify data. Therefore, that all features should exist on the same scale so as to give each feature equal weight in the *k*-means classification process. To meet this requirement, the features (slope, height change, and time duration values) of each segment were transformed by first being log-scaled and then standardized (i.e., by subtracting the mean and dividing by the standard deviation). Scaling and standardizing the data in this way is a common practice for analysis utilizing *k*-means clustering and allows for all features to be considered on the same scale to better suit the Euclidean distance used in *k*-means clustering (Hastie, Tibshirani, and Friedman 2009).

Determining appropriate number of clusters for each dataset: The *k*-value (i.e., number of clusters to use in *k*-means) was determined for positive and negative slopes separately in the **diagnostic mode** of STADIA. This process utilizes the 'gap statistic', which compares the within-cluster dispersion to a null reference distribution when seeking the optimal number of clusters that best separates the data during *k*-means clustering (i.e., the gap statistic answers the question: 'what number of clusters results in the best separation between the clusters?') (Tibshirani, Walther, and Hastie 2001). The gap statistic is the primary driver in determining the proper *k*-value for clustering the line segment data. However, it is also recommended for the user to check how well the number of clusters suggested by the gap statistic describes the dataset qualitatively. Typically, the optimal *k*-value corresponds to the first local maximum

of the gap-statistic plot. In some cases, however, qualitative inspection of the data may suggest that the first local maximum is not optimal, in which case the next local maximum should be used.

For the purposes of informing the optimal *k*-value for use in *k*-means clustering, STADIA repeats clustering procedures for different *k*-values, ranging from 1 through 12, using 100 random starts for each value (*k*-means clustering does not converge to a global maximum so multiple starts are required to determine optimal centroid locations, described below). Simultaneously, STADIA measures the corresponding gap statistic for each value of *k*. As explained above, in our analyses the *k*-value corresponding to the first local maximum of the gap statistic plot was usually chosen as the optimal number of clusters. However, qualitative inspection of the clustering for the positive slopes of the *in vitro* MTs without CLASP2γ and comparison to the other datasets suggested that the first local maximum greater than *k*=1 (i.e., *k*=3) described the data more appropriately.

k-means clustering: Once the optimal number of clusters is determined for both positive and negative slopes using the **diagnostic mode** of STADIA, the user inputs these *k*-values, and *k*-means clustering (Lloyd 1982; Macqueen 1967) is performed in the **fully automated mode** on the positive and negative slopes separately. Segments from simulation data were clustered using *k*=3 for each of the positive and negative slope groups. Similarly, all experimental data (either with or without CLASP2γ) was clustered using *k*=3 for positive slopes and *k*=2 for negative slopes (as discussed in the main text, *k*=2 for negative slopes was appropriate for these datasets because the full depolymerizations were not captured for technical reasons). The final clustering results were obtained from using 500 random starts (again, multiple trials must be performed to determine optimal centroid locations as *k*-means is not guaranteed to converge to a global optimum); centroid locations that attained the lowest sum of squared distances between the centroids and each point in their respective clusters were chosen for further analysis.

Phase bundling: Following *k*-means clustering, the resulting positive and negative sloped clusters are collected, along with the 'flat stutters' that were removed prior to clustering, and all are considered together in the 3-D space defined by the segment features (**SuppMat Figure S7**). Additionally, statistics such as average slopes, average time duration, and average height change are calculated for each cluster and are reported (slopes are illustrated in **Figure 3 C,F** and slopes and time durations are illustrated in **SuppMat Figure S8**). Clusters with similar average slopes are bundled together to form larger groups representing DI phase classes (**Figure 3 I**). Clusters with slopes considerably less in magnitude (flatter) are grouped into a newly identified phase called 'stutters' (along with the 'flat stutters' not considered during the clustering process). The remaining clusters with slopes larger in magnitude (i.e., the higher positive valued and lower negative valued slope segments) more closely resembled the classically understood growth and shortening phases (i.e., similar positively sloped segments would both be considered 'growth' phases, and similar negatively sloped segments would both be considered 'shortening' phases). The name 'stutters' suggests that though there may be micro-level fluctuations in the MT length, the net length does not change considerably over the duration of each stutter segment, especially when compared to segments classified as growth or shortening phases.

At this point, every segment identified during the segmentation stage has been classified as belonging to one of the following DI phase classes: nucleation, growth, shortening, or stutter. Applying these phase class labels to each segment in the length-history plot is illustrated in **Figure 3 G,H**. The chronological ordering of phases, recognized as phase transitions, can now be performed.

Phase and Transition Analysis

After classifying segments into phases, classical methods of calculating DI metrics are adapted for use with the newly identified stutter phases.

Phase analysis: The following attributes of each phase class are calculated: percent time spent in each phase ($\frac{total\ time\ spent\ in\ phase}{total\ time} \times 100\%$), total number of segments (from the piecewise linear approximation) for each phase, and percent height change corresponding to each phase (**Figure 4 A** and **SuppMat Figure S9**).

Transition analysis: Transition frequencies are calculated in a manner similarly to what has been done classically. However, with the newly identified stutter phases, there are additional transitions to consider. In particular, it is necessary to determine whether catastrophes and rescues are (or are not) directly preceded by stutters. Catastrophes and rescues are identified as either abrupt (occurring without detectable stutters) or transitional (occurring via a stutter) (**Figure 4 D,E,F,G and Figure 5 D,E,F,G**). Additionally, our analysis quantifies interrupted growth (growth → stutter → growth) (**Figure 4 H; Figure 5 H,I**) and interrupted shortening (shortening → stutter → shortening) (**Figure 4 I**). Note that MTs shorter than a user-defined threshold (here the threshold used was 75 dimer lengths) are considered to be in 'nucleation' phase; transitions into or out of nucleation phases are not considered here because such MTs would be difficult to detect in experiments, and their behavior might be influenced by the seed.

In agreement with what has been done in classic DI analyses, frequencies of catastrophe and rescue are calculated as the ratio of the number of catastrophe or rescue events to the total time spent in growth or shortening, respectively (**Table 1; SuppMat Figure S9**). Similarly, interruptions are calculated as the ratio of the number of interrupted growths or interrupted shortenings to the total time spent in growth or shortening, respectively. Calculations can be done separately for abrupt and transitional types (e.g., $F_{\text{Abrupt Catastrophe}} = \frac{\#\ of\ abrupt\ catastrophes}{total\ time\ spent\ in\ growth}$) or collectively by simply adding the frequencies for each type together ($F_{cat} = F_{\text{abrupt catastrophe}} + F_{\text{transitional catastrophe}}$) (**SuppMat Figure S9**).

For other information including the data acquisition methods for both the *in silico* and the *in vitro* experiments, please see the Supplemental Material.

REFERENCES

Aher, Amol, Maurits Kok, Ashwani Sharma, Michel O Steinmetz, Marileen Dogterom, and Anna Akhmanova. 2018. "CLASP Suppresses Microtubule Catastrophes through a Single TOG Domain." *Developmental Cell* 46 (1): 40–58. https://doi.org/10.1016/j.devcel.2018.05.032.

Castle, Brian T, and David J Odde. 2013. "Brownian Dynamics of Subunit Addition-Loss Kinetics and Thermodynamics in Linear Polymer Self-Assembly." *Biophysical Journal* 105 (11): 2528–40. https://doi.org/10.1016/j.bpj.2013.10.009.

Coombes, Courtney E., Ami Yamamoto, Madeline R. Kenzie, David J. Odde, and Melissa K. Gardner. 2013. "Evolving Tip Structures Can Explain Age-Dependent Microtubule Catastrophe." *Current Biology* 23 (14): 1342–48. https://doi.org/10.1016/j.cub.2013.05.059.

Desai, Arshad, and Timothy J. Mitchison. 1997. "Microtubule Polymerization Dynamics." *Annual Review of Cell and Developmental Biology* 13 (1): 83–117. https://doi.org/10.1146/annurev.cellbio.13.1.83.

Doodhi, Harinath, Andrea E Prota, Ruddi Rodríguez-García, Lukas C Kapitein, Anna Akhmanova, and Michel O Steinmetz. 2016. "Termination of Protofilament Elongation by Eribulin Induces Lattice Defects That Promote Microtubule Catastrophes." *Current Biology* 26 (13): 1713–21. https://doi.org/10.1016/j.cub.2016.04.053.

Duellberg, Christian, Nicholas I Cade, David Holmes, and Thomas Surrey. 2016. "The Size of the EB Cap Determines Instantaneous Microtubule Stability." *ELife* 5 (April). https://doi.org/10.7554/eLife.13470.

Duellberg, Christian, Nicholas Ian Cade, and Thomas Surrey. 2016. "Microtubule Aging Probed by Microfluidics-Assisted Tubulin Washout." *Molecular Biology of the Cell* 27 (22): 3563–73. https://doi.org/10.1091/mbc.E16-07-0548.

Gildersleeve, R F, A R Cross, K E Cullen, A P Fagen, and R C Williams. 1992. "Microtubules Grow and Shorten at Intrinsically Variable Rates." *The Journal of Biological Chemistry* 267 (12): 7995–8006. http://www.ncbi.nlm.nih.gov/pubmed/1569058.

Goodson, Holly V., and Erin M. Jonasson. 2018. "Microtubules and Microtubule-Associated Proteins." *Cold Spring Harbor Perspectives in Biology* 10 (6): a022608. https://doi.org/10.1101/cshperspect.a022608.

Guo, Yuting, Di Li, Siwei Zhang, Yanrui Yang, Jia-Jia Liu, Xinyu Wang, Chong Liu, et al. 2018. "Visualizing Intracellular Organelle and Cytoskeletal Interactions at Nanoscale Resolution on Millisecond Timescales." *Cell* 175 (5): 1430-1442.e17. https://doi.org/10.1016/j.cell.2018.09.057.

Hastie, Trevor, Robert Tibshirani, and Jerome Friedman. 2009. *Springer Series in Statistics: The Elements of Statistical Learning*. *Springer*. https://doi.org/10.1007/b94608.

Jonasson, Erin M., Ava J. Mauro, Chunlei Li, Ellen C. Labuz, Shant M. Mahserejian, Jared P. Scripture, Ivan V. Gregoretti, Mark Alber, and Holly V. Goodson. 2019. "Behaviors of Individual Microtubules and Microtubule Populations Relative to Critical Concentrations: Dynamic Instability Occurs When Critical Concentrations Are Driven Apart by Nucleotide Hydrolysis." *Molecular Biology of the Cell*, October, mbc.E19-02-0101. https://doi.org/10.1091/mbc.e19-02-0101.

Lawrence, E. J., and M. Zanic. 2019. "Rescuing Microtubules from the Brink of Catastrophe: CLASPs Lead the Way." *Current Opinion in Cell Biology* 56 (February): 94–101. https://doi.org/10.1016/j.ceb.2018.10.011.

Lawrence, Elizabeth J., Göker Arpag, Stephen R. Norris, and Marija Zanic. 2018. "Human CLASP2 Specifically Regulates Microtubule Catastrophe and Rescue." *Molecular Biology of the Cell* 29 (10): 1168–77. https://doi.org/10.1091/mbc.E18-01-0016.

Lloyd, Stuart P. 1982. "Least Squares Quantization in PCM." *IEEE Transactions on Information Theory* 28 (2): 129–37. https://doi.org/10.1109/TIT.1982.1056489.

Macqueen, J. 1967. "Some Methods for Classification and Analysis." In *Proceedings of the Fifth Berkeley Symposium on Mathematical Statistics and Probability, Volume 1: Statistics*, 233:281–97.

http://citeseer.ist.psu.edu/viewdoc/summary?doi=10.1.1.308.8619.

Majumdar, Shreoshi, Tae Kim, Zhe Chen, Sarah Munyoki, Shih-Chia Tso, Chad A. Brautigam, and Luke M. Rice. 2018. "An Isolated CLASP TOG Domain Suppresses Microtubule Catastrophe and Promotes Rescue." Edited by Thomas Surrey. *Molecular Biology of the Cell* 29 (11): 1359–75. https://doi.org/10.1091/mbc.E17-12-0748.

Margolin, Gennady, Ivan V Gregoretti, Trevor M Cickovski, Chunlei Li, Wei Shi, Mark S Alber, and Holly V Goodson. 2012. "The Mechanisms of Microtubule Catastrophe and Rescue: Implications from Analysis of a Dimer-Scale Computational Model." *Molecular Biology of the Cell* 23 (4): 642–56. https://doi.org/10.1091/mbc.E11-08-0688.

Maurer, Sebastian P., Nicholas I. Cade, Gergö Bohner, Nils Gustafsson, Emmanuel Boutant, and Thomas Surrey. 2014. "EB1 Accelerates Two Conformational Transitions Important for Microtubule Maturation and Dynamics." *Current Biology* 24 (4): 372–84. https://doi.org/10.1016/j.cub.2013.12.042.

Mitchison, Tim, and Marc Kirschner. 1984. "Dynamic Instability of Microtubule Growth." *Nature* 312 (5991): 237–42. https://doi.org/10.1038/312237a0.

Moriwaki, Takashi, and Gohta Goshima. 2016. "Five Factors Can Reconstitute All Three Phases of Microtubule Polymerization Dynamics." *The Journal of Cell Biology* 215 (3): 357–68. https://doi.org/10.1083/jcb.201604118.

Pedigo, Susan, and Robley C Williams. 2002. "Concentration Dependence of Variability in Growth Rates of Microtubules." *Biophysical Journal* 83 (4): 1809–19. https://doi.org/10.1016/S0006-3495(02)73946-5.

Pham, D T, S S Dimov, and C D Nguyen. 2005. "Selection of K in K-Means Clustering." *Proceedings of the Institution of Mechanical Engineers, Part C: Journal of Mechanical Engineering Science* 219 (1): 103–19. https://doi.org/10.1243/095440605X8298.

Rickman, Jamie, Christian Duellberg, Nicholas I Cade, Lewis D Griffin, and Thomas Surrey. 2017. "Steady-State EB Cap Size Fluctuations Are Determined by Stochastic Microtubule Growth and Maturation." *Proceedings of the National Academy of Sciences of the United States of America* 114 (13): 3427–32. https://doi.org/10.1073/pnas.1620274114.

Sousa, Aureliana, Rita Reis, Paula Sampaio, and Claudio E. Sunkel. 2007. "The *Drosophila* CLASP Homologue, Mast/Orbit Regulates the Dynamic Behaviour of Interphase Microtubules by Promoting the Pause State." *Cell Motility and the Cytoskeleton* 64 (8): 605–20. https://doi.org/10.1002/cm.20208.

Steinley, Douglas. 2006. "K-Means Clustering: A Half-Century Synthesis." *British Journal of Mathematical and Statistical Psychology* 59 (1): 1–34. https://doi.org/10.1348/000711005X48266.

Tibshirani, Robert, Guenther Walther, and Trevor Hastie. 2001. "Estimating the Number of Clusters in a Data Set via the Gap Statistic." *Journal of the Royal Statistical Society: Series B (Statistical Methodology)* 63 (2): 411–23. https://doi.org/10.1111/1467-9868.00293.

Walker, R. A., E. T. O'Brien, N. K. Pryer, M. F. Soboeiro, W. A. Voter, H. P. Erickson, and E. D. Salmon. 1988. "Dynamic Instability of Individual Microtubules Analyzed by Video Light Microscopy: Rate Constants and Transition Frequencies." *The Journal of Cell Biology* 107 (4): 1437–48. https://doi.org/10.1083/jcb.107.4.1437.

Yenjerla, Mythili, Manu Lopus, and Leslie Wilson. 2010. "Analysis of Dynamic Instability of Steady-State Microtubules In Vitro by Video-Enhanced Differential Interference Contrast Microscopy with an Appendix by Emin Oroudjev." *Methods in Cell Biology* 95: 189–206. https://doi.org/10.1016/S0091-679X(10)95011-5.

Zanic, Marija. 2016. "Measuring the Effects of Microtubule-Associated Proteins on Microtubule Dynamics In Vitro." In *The Mitotic Spindle*, 47–61. https://doi.org/10.1007/978-1-4939-3542-0_4.

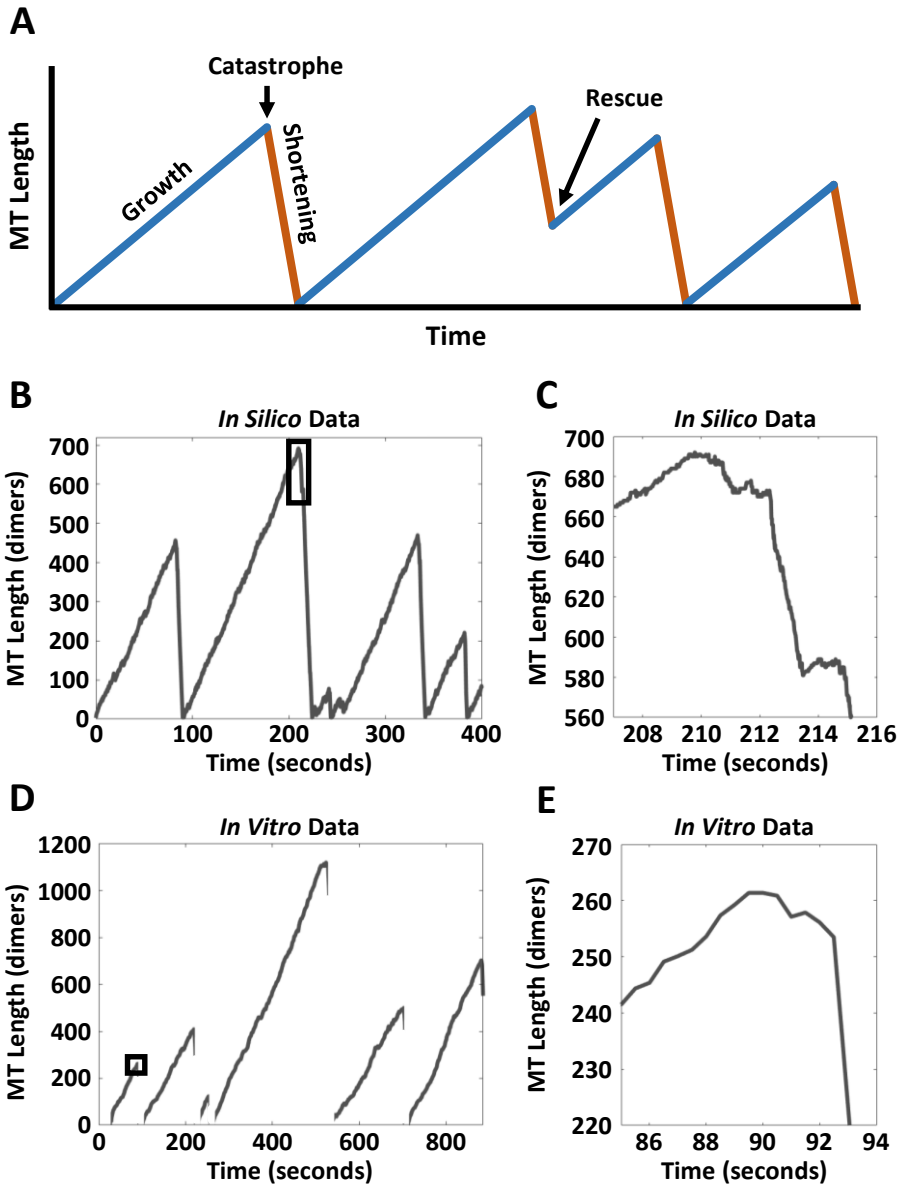

Figure 1. Qualitative examples of behavior that does not fit two-state framework in high-resolution simulation (*in silico*) and experimental (*in vitro*) data. (A) An illustration of the classically recognized two-state representation of DI, recognizing behavior as simply growth and shortening phases, with instantaneous transitions known as catastrophe and rescue events. **(B,D)** Zoomed out (two-state representation analogous to (A)) length history plots of simulation data (detailed 13-PF model; see Methods) and experimental data (note that depolymerizations were not tracked in their entirety in these experiments). Black rectangles in B (simulation data) and D (experimental data) indicate the zoomed-in portions shown in C and E, respectively. **(C,E)** Closer inspection of transitions shows ambiguous behavior that cannot clearly be categorized as either growth or shortening. Other behavioral phases need to be considered in order to fully describe MT transitions and identify the exact moments where transitions occur.

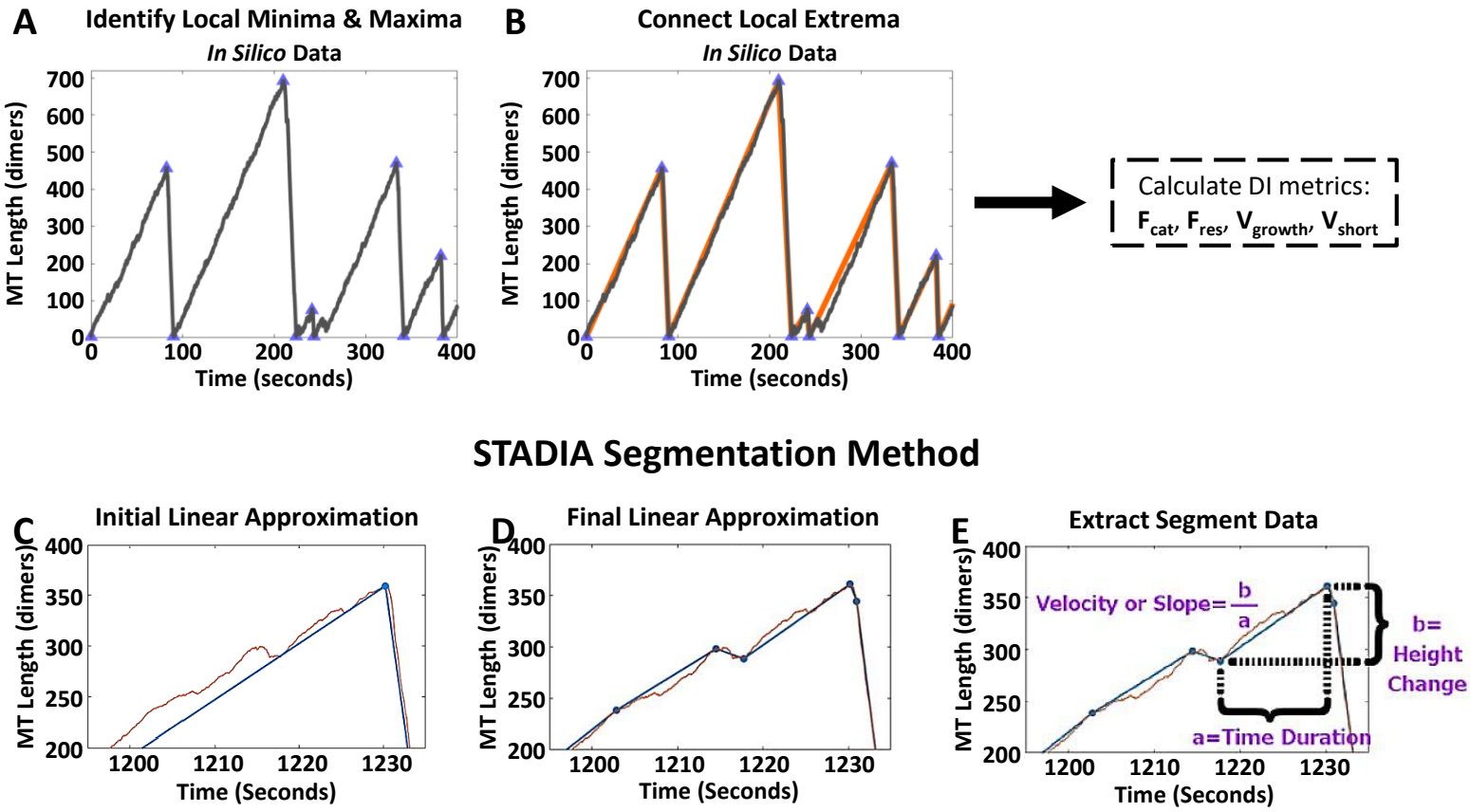

Figure 2. Continuous piecewise linear approximation of length history data & segment data extraction. *Classical Segmentation Method*: (A) Identify major vertices, such that local maxima and minima (blue triangles) are considered as catastrophes and rescues (or nucleation events) respectively. **(B)** Connect major vertices (orange lines) to create a segmentation and approximation of the MT length history data. Then calculate DI metrics from this approximation. ***STADIA Segmentation Method*: (C)** Generate initial approximation by finding major peaks and valleys (local extrema with high prominence) and connecting these with line segments. **(D)** Iteratively include new vertices (blue dots) where the highest error occurs in each segment to produce the final approximation, such that all point-wise errors are less than the user-defined threshold (usually 10 to 25 dimer subunits). Note: this method produces a closer approximation of the data than the classical segmentation method produces. **(E)** Calculate slope, height change, and time duration for each segment, and use for *K*-means clustering during the classification stage of STADIA.

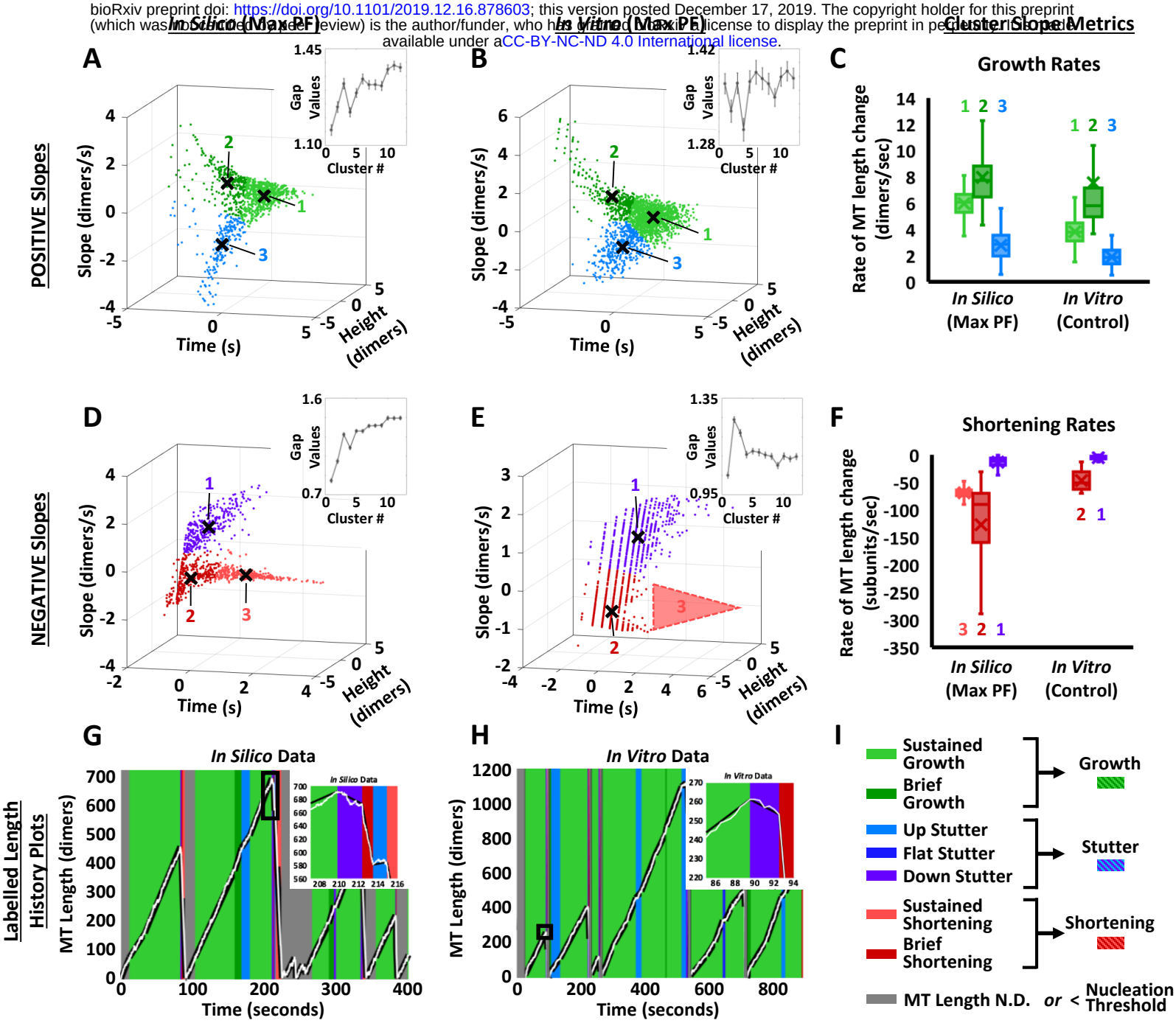

Figure 3. Cluster analysis results, slope metrics for the different clusters across data sets, and subsets of length history data with subsequently labeled DI phases. STADIA performs the cluster analysis using the segment-feature metrics (slope, height change, and time duration) identified in the length history approximation during the segmentation stage. (A,B) Log-transformed and standardized segment features extracted from *in silico* and *in vitro* (control, no CLASP2γ) length history data approximations for positive sloped line segments. Three clusters are suggested by the gap statistic for positive slopes in both data sets. **(D,E)** Log-transformed and standardized segment features extracted from *in silico* and *in vitro* (control, no CLASP2γ) length history data approximations for negative sloped line segments. The gap statistic suggested 3 clusters for the *in silico* negative sloped segments and 2 clusters for the *in vitro* negative sloped segments. **(C,F)** Growth rates for the positive sloped segment clusters and shortening rates for negative sloped segment clusters identified in the *in silico* and *in vitro* data sets. For positive slopes in each data set, two clusters (light and dark green) had average growth rates relatively large in magnitude compared to the third (light blue). For negative slopes in each data set, the red (and light red for *in silico* data) labeled shortening rates were on average relatively large in magnitude compared to the purple labeled group. **(G,H)** Previously unlabeled *in silico* and *in vitro* MT length history plots (see Figure 1 A,C) are now labeled according to the subgroups that each line segment fits into. Zoomed-in portions of previously ambiguous length history data (see Figure 1 B,D) are now clearly labeled as well-defined DI phases. **(I)** Examination of the average slopes of the individual clusters indicates that bundling subgroups (clusters) together into larger phase classes based on the average slopes of the individual clusters is appropriate. Clusters with positive and negative slopes relatively larger in magnitude were bundled together into 'Growth' and 'Shortening' phases respectively. The remaining clusters, where significantly less changes in length occur, were bundled together, along with the previously identified 'near zero' slope or flat segments, into a new phase called 'Stutters'. Further, 'Brief' and 'Sustained' sub-classes of the Growth and Shortening phases were characterized by their time durations. The 'Up', 'Flat', and 'Down' sub-classes of the Stutter phase are characterized by the segment slope being positive, near-zero, or negative, respectively.

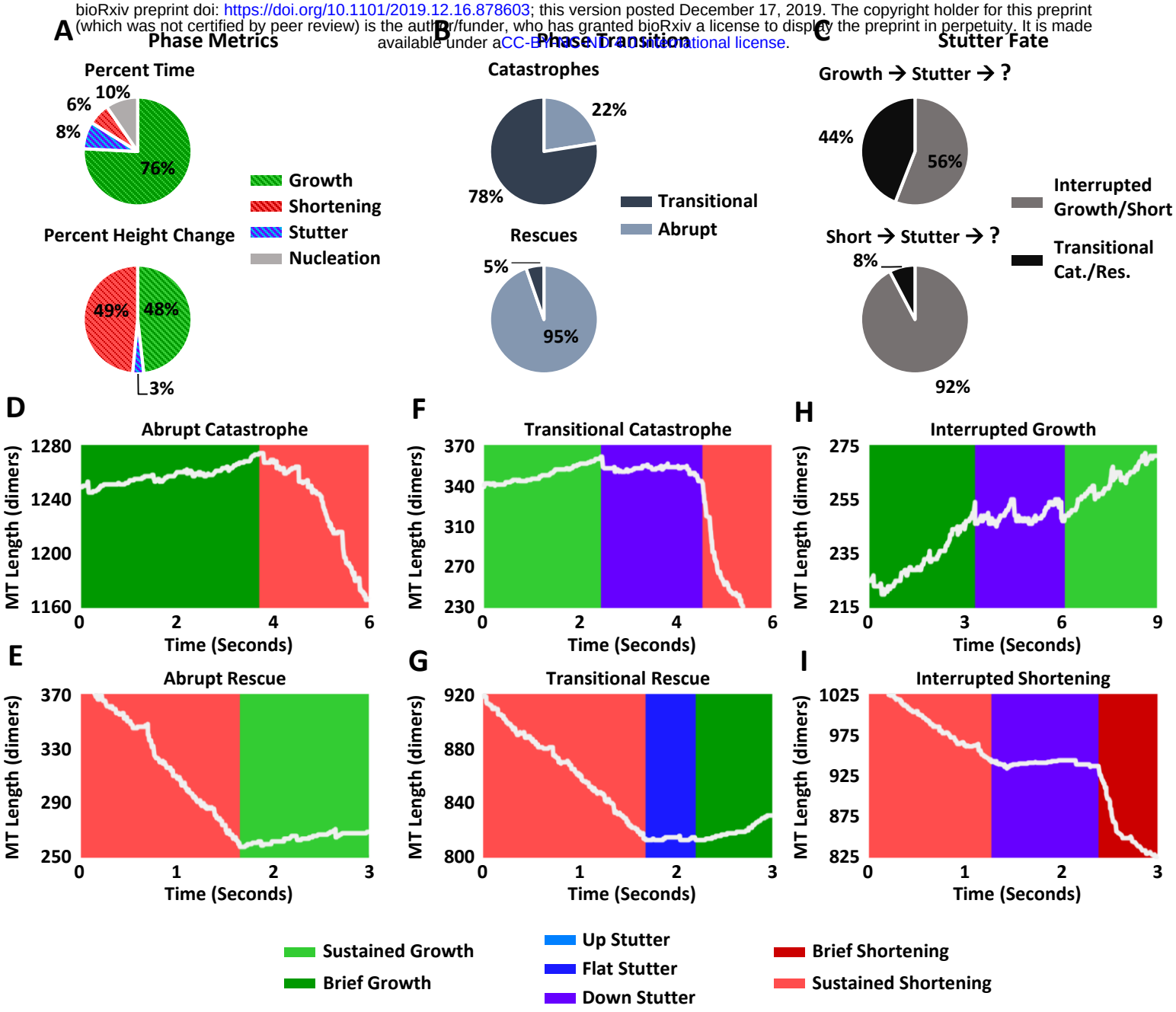

Figure 4. Phase metrics and transition analysis for *in silico* data (Max Protofilament length). (A) Percent time spent in and percent height (MT length) change occurring during each bundled phase. A large majority of time is spent in the growth phase. Interestingly, *in silico* MTs spend more time in the stutter phase than in the shortening phase, thus making stutters a significant phase worth studying. Most height change occurs during growth and shortening phases, as is expected. Stutters account for a markedly smaller percentage of height change, particularly when considered relative to their percentage of time; this makes sense given that little height change takes place during stutter segments. **(B)** Percentages of transitional vs. abrupt phase changes (transitional = with stutter phase between the growth/shortening phases; abrupt = without stutters) to/from growth and shortening show that catastrophes are primarily transitional, whereas rescues are overwhelmingly abrupt. **(C)** The percentage of phase transitions with stutters are compared separately for growth-to-stutters transitions and shortening-to-stutter transitions. A bit more than half of the transitions entering stutters from a growth phase were observed to return to a growth phase; in other words, stutter phases occur somewhat more commonly in interrupted growth transitions than transitional catastrophes. A vast majority of transitions entering stutters from a shortening phase return to shortening, i.e., stutter phases appear in interrupted shortening transitions much more commonly than transitional rescues. **(D,E,F,G)** Examples of abrupt/transitional catastrophes (D,F) and abrupt/transitional rescues (E,G) for *in silico* MTs. Background colors indicate the subgroup identified by STADIA for various sections of length history data. **(H,I)** Examples of interrupted growth and interrupted shortening for *in silico* MTs, where interruption is defined by MTs in a growth/shortening phase undergoing a transition into a stutter phase, and then returning to growth/shortening (growth-stutter-growth or shortening-stutter-shortening).

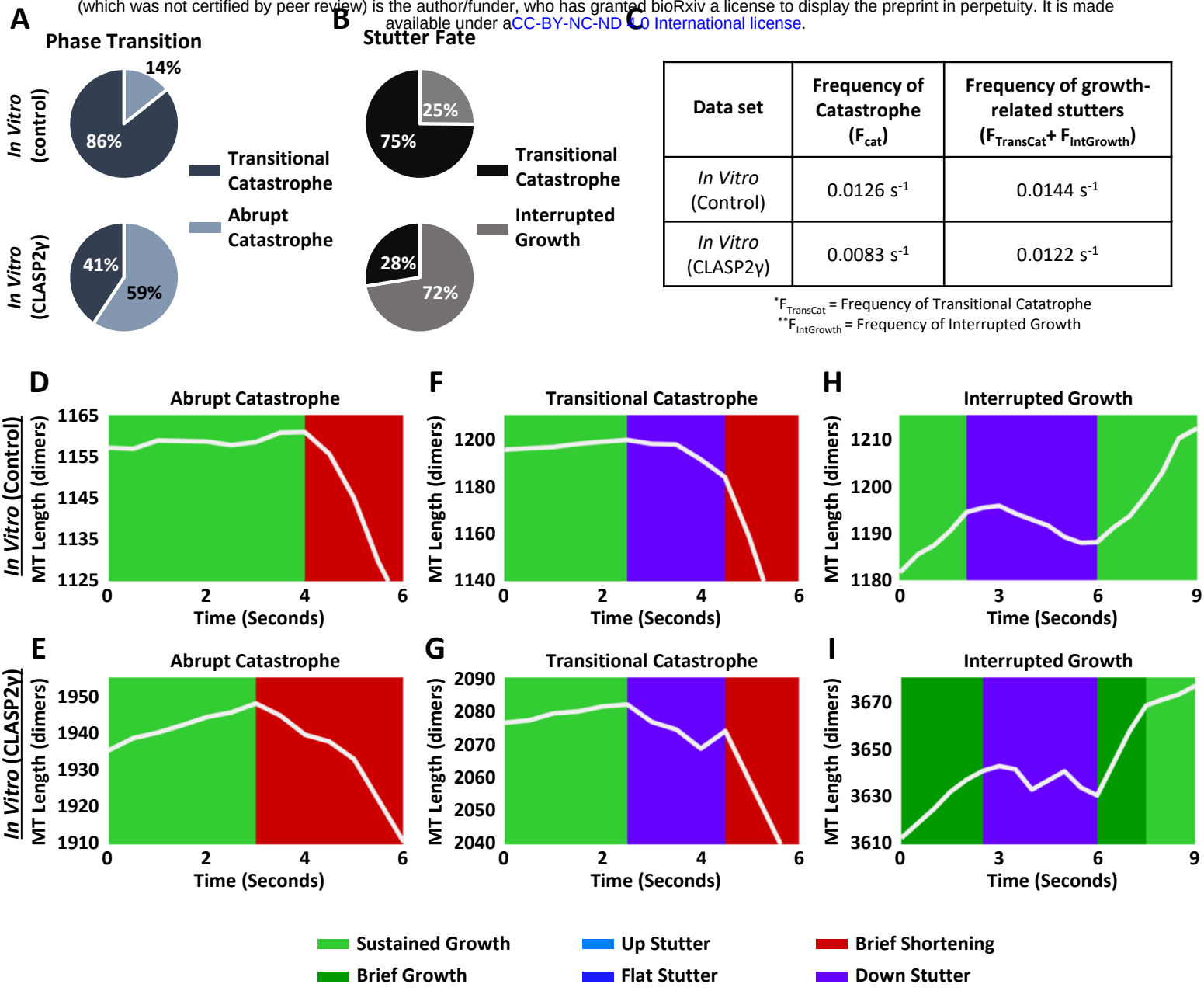

Data set	Frequency of Catastrophe (F_{cat})	Frequency of growth-related stutters ($F_{TransCat}$+ $F_{IntGrowth}$)
In Vitro (Control)	0.0126 s^{-1}	0.0144 s^{-1}
In Vitro (CLASP2γ)	0.0083 s^{-1}	0.0122 s^{-1}

*$F_{TransCat}$ = Frequency of Transitional Catatrophe
**$F_{IntGrowth}$ = Frequency of Interrupted Growth

Figure 5. Effect of CLASP2γ on the nature of catastrophes and the fate of MTs entering stutter phase. (A) Consistent with what was seen for *in silico* MTs, the majority of catastrophes for *in vitro* MTs without CLASP2γ are transitional. In contrast, introduction of CLASP2γ results in a reduction of stutter phases preceding catastrophes; it is possible that this is due to CLASP2γ promoting growth after stutter phases. **(B)** When MTs transition from growth to stutter phases, they are more likely to transition into a depolymerization phase when CLASP2γ is not present (i.e., without CLASP2γ, transitional catastrophes occur more often than interrupted growth). With CLASP2γ, however, when MTs move from growth to stutter phases, they are more likely to transition back into the growth phase (i.e., with CLASP2γ, interrupted growth occurs more often than transitional catastrophes). These results provide a possible explanation for how CLASP2γ changes the overall makeup of catastrophes for *in vitro* MTs: transitions that would have been transitional catastrophes without CLASP2γ are now interrupted growths with CLASP2γ. **(C)** CLASP2γ decreases the overall frequency of catastrophe without significantly reducing the frequency of transitioning from the growth phase to the stutter phase, indicating that CLASP2γ is preventing catastrophes by promoting growth following stutters without preventing stutters altogether. **(D,E,F,G)** Examples of transitional and abrupt catastrophes, for *in vitro* MTs both with (bottom) and without (top) CLASP2γ, show a clear qualitative distinction between transitional and abrupt catastrophes identified by STADIA. **(H,I)** Examples of interrupted growth exhibited by *in vitro* MTs both with (bottom) and without (top) CLASP2γ shows a transition from growth into stutter and back into growth phase.

Comparison of Full Analysis to k=1 and Classical Method

Simulation Data (Max PF Length)						
Method	**Total Cat.**	**Total Res.**	**F_{cat} (min^{-1})**	**F_{res} (min^{-1})**	**V_{growth} (nm/s)**	**V_{short} (nm/s)**
Classical Method	355	123	0.659	2.483	46.1 ± 5.1	540.0 ± 47.9
Strictly two-state: *k=1 for pos & neg	449	214	0.912	4.391	46.4 ± 18.4	530.4 ± 556.0
Two-state w/ flat stutters: **k=1 for pos & neg	429	195	0.870	4.098	47.2 ± 17.6	547.2 ± 556.8
All phases found by STADIA: k=3 pos, k=3 neg	298	75	0.660	1.944	48.0 ± 7.2 63.2 ± 19.2 22.4 ± 8.8	552.8 ± 87.2 1016.8 ± 717.6 107.2 ± 72.8

Experimental Data (Control)						
Method	**Total Cat.**	**Total Res.**	**F_{cat} (min^{-1})**	**F_{res} *** (min^{-1})**	**V_{growth} (nm/s)**	**V_{short} **** (nm/s)**
Classical Method	802	40	0.717	N.D.	29.5 ± 12.7	330.1 ± 136.5
Strictly two-state: *k=1 for pos & neg	856	83	0.777	N.D.	32.0 ± 24.8	216 ± 199.2
Two-state w/ flat stutters: **k=1 for pos & neg	846	76	0.760	N.D.	32.8 ± 24.8	227.2 ± 198.4
All phases found by STADIA: k=3 pos, k=2 neg	734	18	0.756	N.D.	30.4 ± 7.2 60.0 ± 44.8 15.2 ± 5.6	373.6 ± 143.2 39.2 ± 25.6

Experimental Data (CLASP2γ)						
Method	**Total Cat.**	**Total Res.**	**F_{cat} (min^{-1})**	**F_{res} *** (min^{-1})**	**V_{growth} (nm/s)**	**V_{short} **** (nm/s)**
Classical Method	99	62	0.500	N.D.	43.1 ± 34.4	155.1 ± 77.6
Strictly two-state: *k=1 for pos & neg	142	94	0.720	N.D.	46.4 ± 41.6	96.0 ± 84.0
Two-state w/ flat stutters: **k=1 for pos & neg	131	87	0.676	N.D.	48.0 ± 41.6	108 ± 82.4
All phases found by STADIA: k=3 pos, k=2 neg	86	52	0.498	N.D.	37.6 ± 11.2 100.0 ± 57.6 16.0 ± 7.2	158.4 ± 68.8 32.8 ± 17.6

Sustained Growth
Brief Growth
Up Stutter
Down Stutter
Sustained Shortening
Brief Shortening

Table 1. Comparison of DI metrics from classical two-state analysis, STADIA two-state analysis, and STADIA full analysis. The results from the full, automated analysis conducted by STADIA were compared to results from both the classical method (identifying only major peaks and valleys, and connecting line segments to form a course-grained approximation) as well as two-state approaches (a fine-grained approximation was generated by STADIA, but phase classes were restricted to only growth and shortening (*) or growth, shortening, and flat stutters (**)). While there is not one-to-one correspondence between any of the methods, there is general agreement where possible. For the experimental datasets, depolymerizations were not captured in their entirety, so (***) rescue data was not reported and (****) negative slope segments were separated into only two clusters, yielding only two V_{short} measurements. V_{growth} and V_{short} measurements are listed in a mean ± standard deviation format. Additionally, rescue metrics were not determined (N.D.) for experimental data due to depolymerizations not being captured in their entirety.

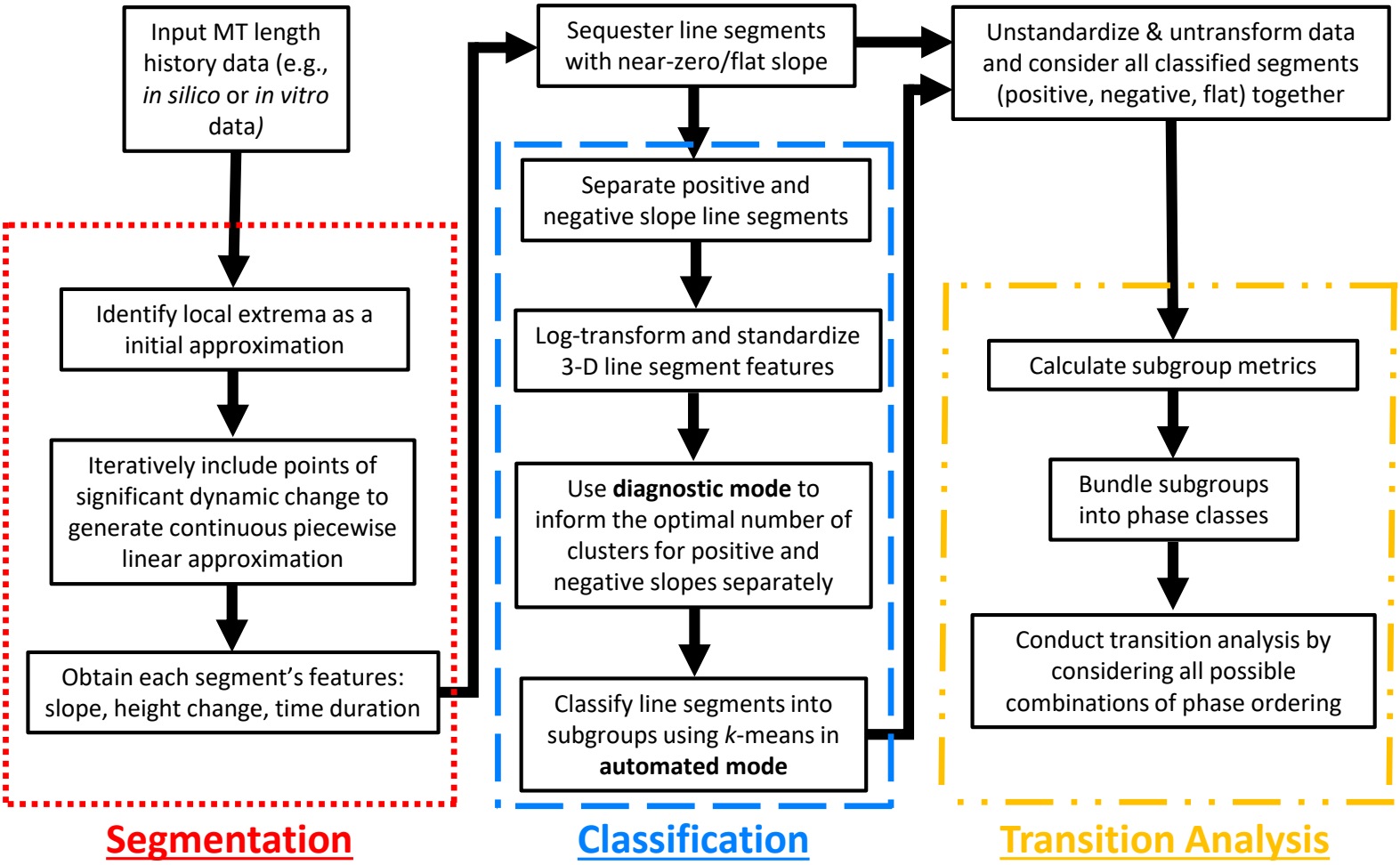

Figure S1. Workflow diagram outlining main steps of STADIA.

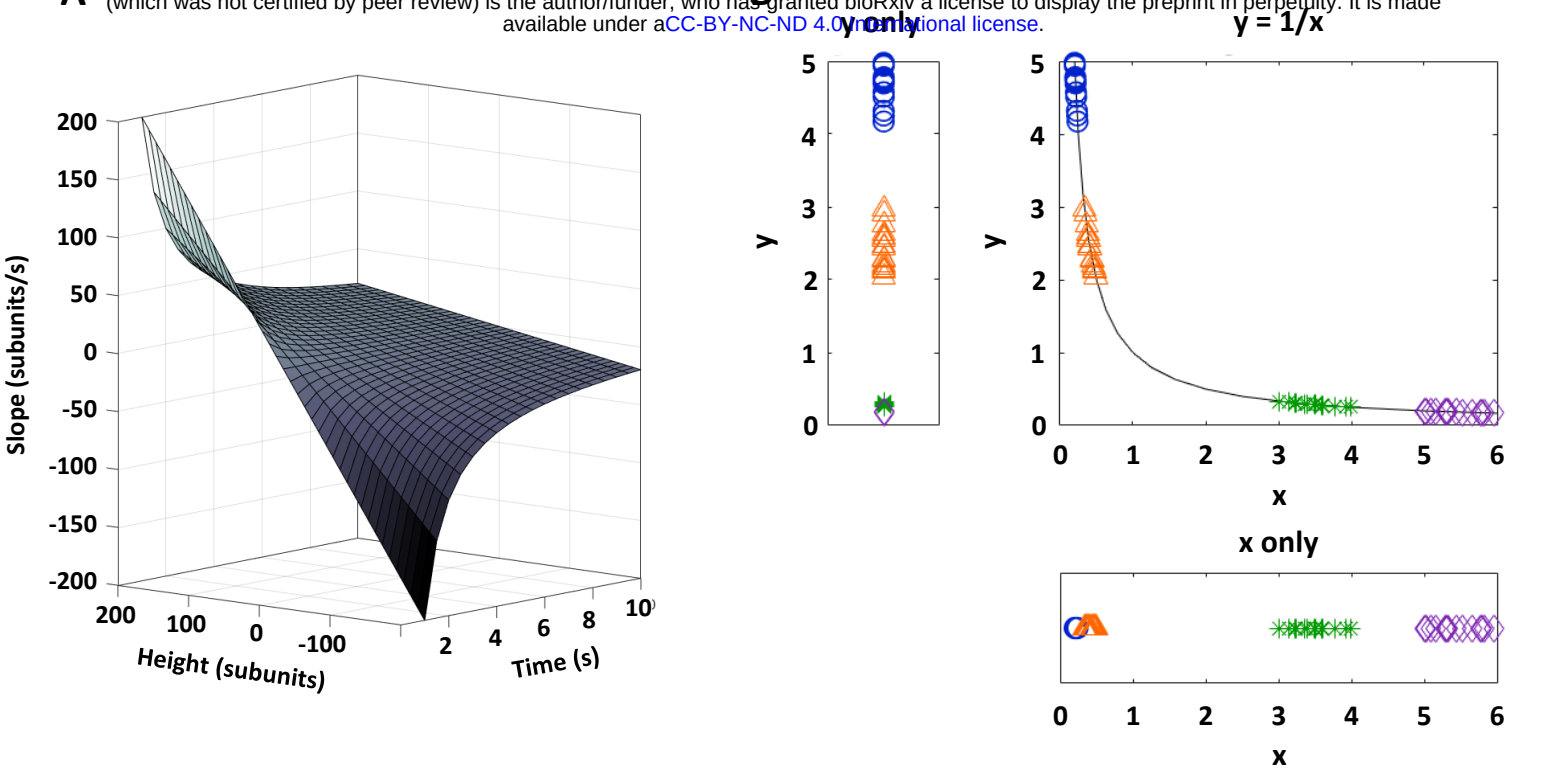

Figure S2. (A) Data points representing each line segment reside on this Z(X,Y) = X/Y manifold, where Z = slope, X = time, and Y = height. **(B)** Justification for using height, time, and slope is demonstrated using a parallel example in two dimensions where we plot a dataset containing four groups (clusters) of points that fall on the curve determined by the function y = 1/x. Plotting only y (top left) or only x (bottom right) creates the appearance that this dataset contains only three groups of points. In contrast, when the data are plotted in two dimensions (upper right), the data are separated sufficiently to reveal that the dataset actually contains four groups of points. For similar reasons, we need to consider all three variables in our line segment data to properly identify the groups in our dataset.

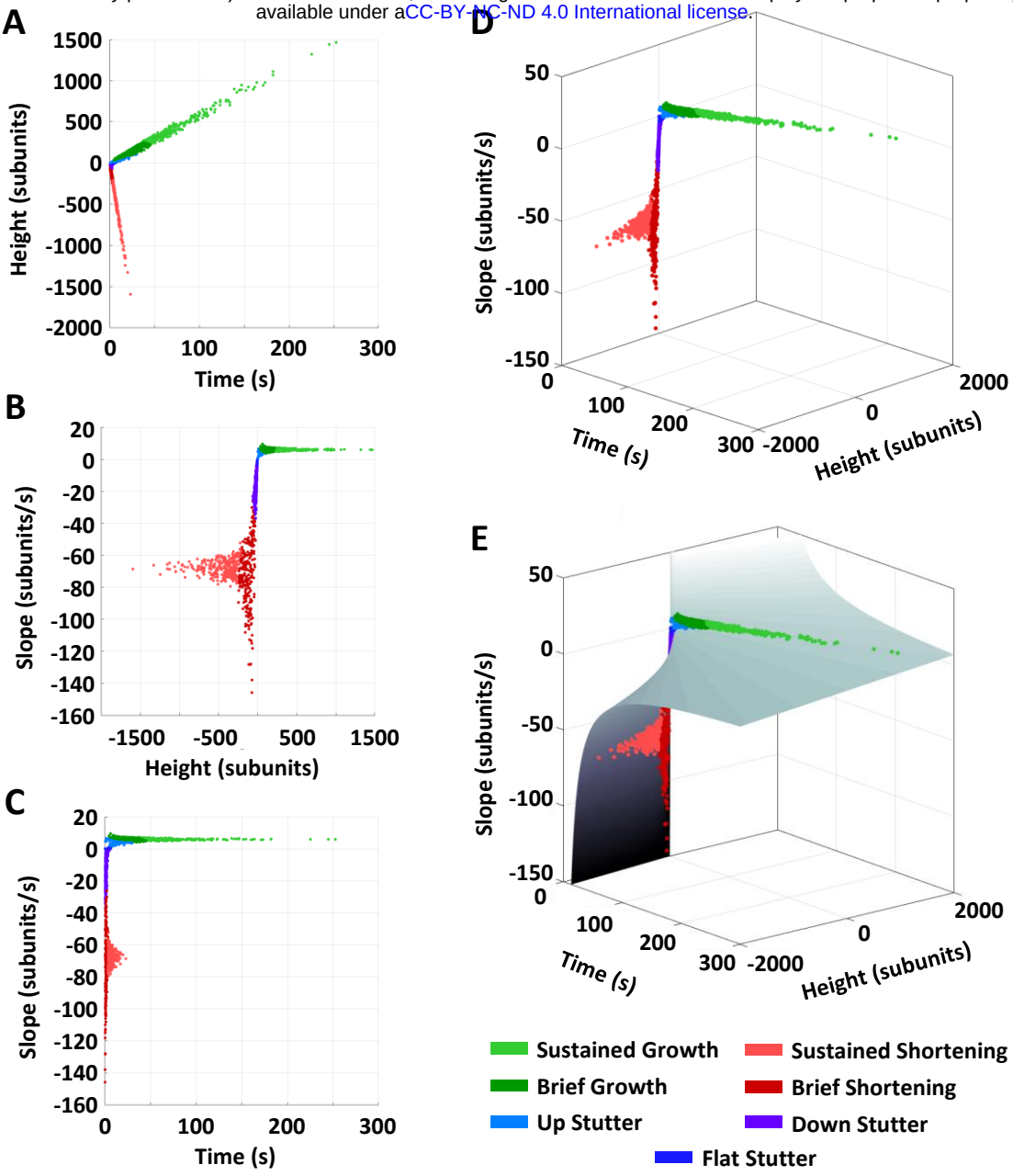

Figure S3. The segment features (slope, height change, and time duration) for segments identified from the piecewise linear approximation to the *in silico* length history data. Each point corresponds to one line segment from the length history approximation and is colored according to the phase class identified by STADIA after a full analysis. **(A-D)** Multiple perspectives of the same plot, provided to help visualize the 3-D data. **(E)** An illustration of how the segment points lie on the Z=Y/X manifold described in Supplemental Figure S2.

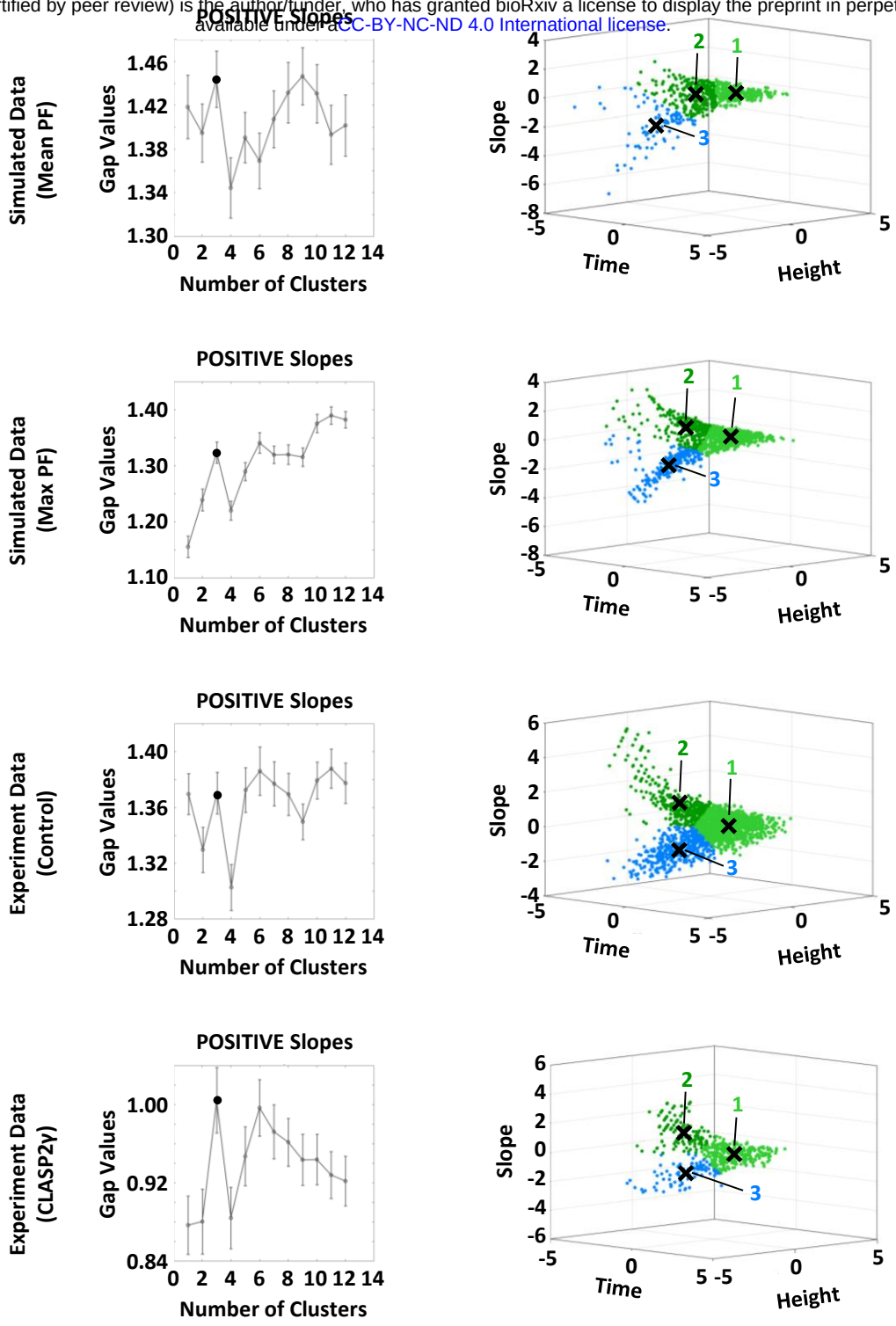

Figure S4. Gap Statistic plots and corresponding clustering profiles for positive slope segments in each log transformed and normalized data set. When using the gap statistic to suggest the best number of clusters to use in *k*-means clustering, the rule of thumb is to use the first *k*-value where the gap statistic plot shows a local maximum. In practice here, we expect the number of clusters to be greater than 1, because the 3-D data structure shows multiple appendages separated by a sparsely populated region of points. Thus, for the case with simulation data using the mean PF length and the control experimental data, the local maximum at *k*=1 is rejected. Taking this into consideration, all data sets indicate that the gap statistic attains the first local maximum greater than one at *k*=3. So, for all positive slope segment data, *k*-means clustering is performed by separating the data into 3 clusters. Furthermore, since the clustering profile of the simulation data using the max PF length more closely resembles the clustering profile of the experimental data, we choose to use the max PF data instead of the mean PF data for presenting the STADIA results in the main text.

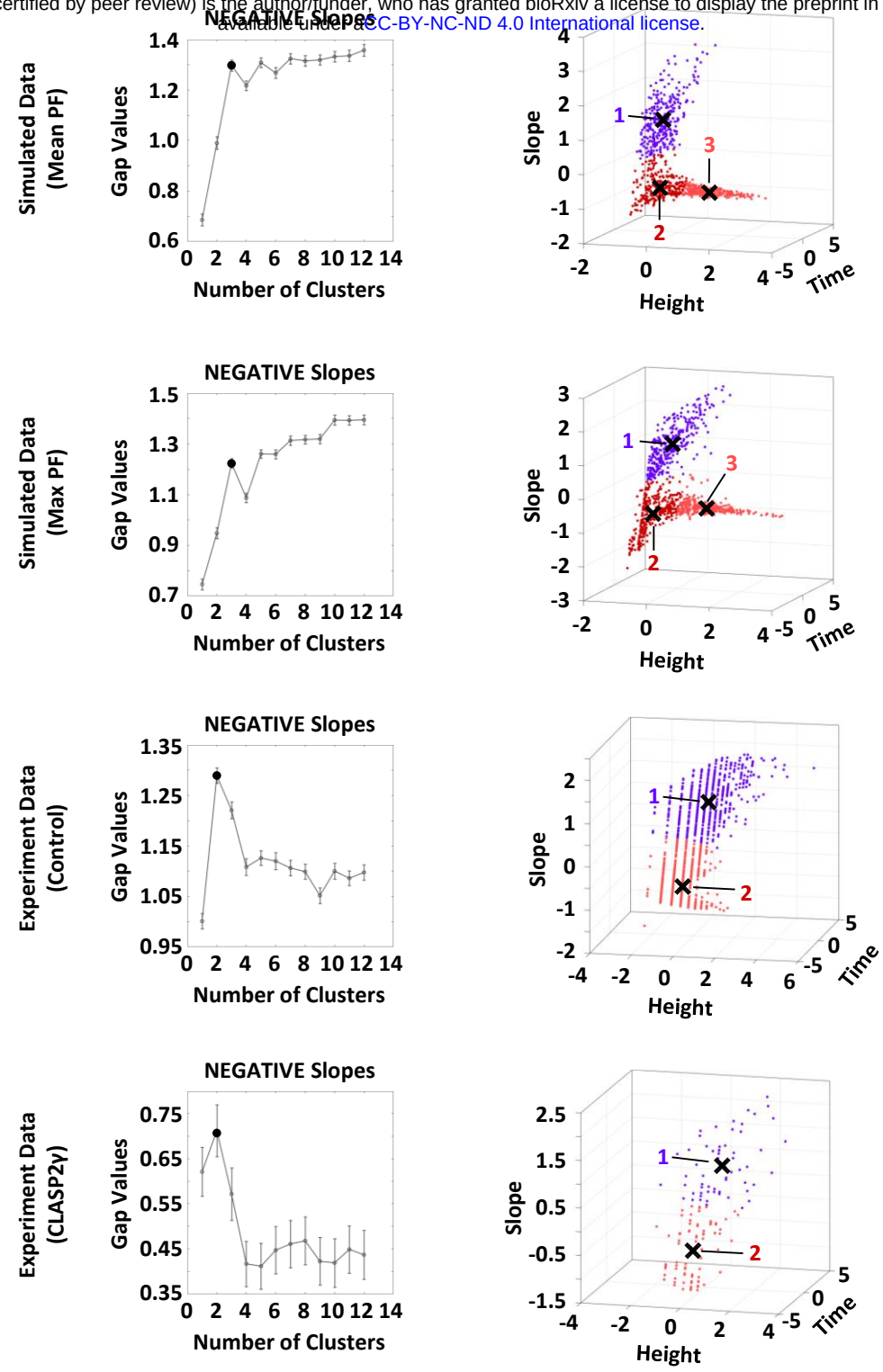

Figure S5. Gap Statistic plots and corresponding clustering profiles for negative slope segments in each log transformed and normalized data set. When using the gap statistic to suggest the best number of clusters to use in *k*-means clustering, the rule of thumb is to use the first *k*-value where the gap statistic plot shows a local maximum. The two simulation data sets indicate that the gap statistic attains the first local maximum greater than one at *k*=3, whereas the experimental data sets indicate *k*=2. We attribute this disagreement to the fact that in these experimental datasets, only the beginnings of depolymerization events were captured, thus omitting long time duration shortening segments from the dataset. So, for negative slope segments, we performed *k*-means clustering separating the simulation data into 3 clusters and the experimental data into 2 clusters.

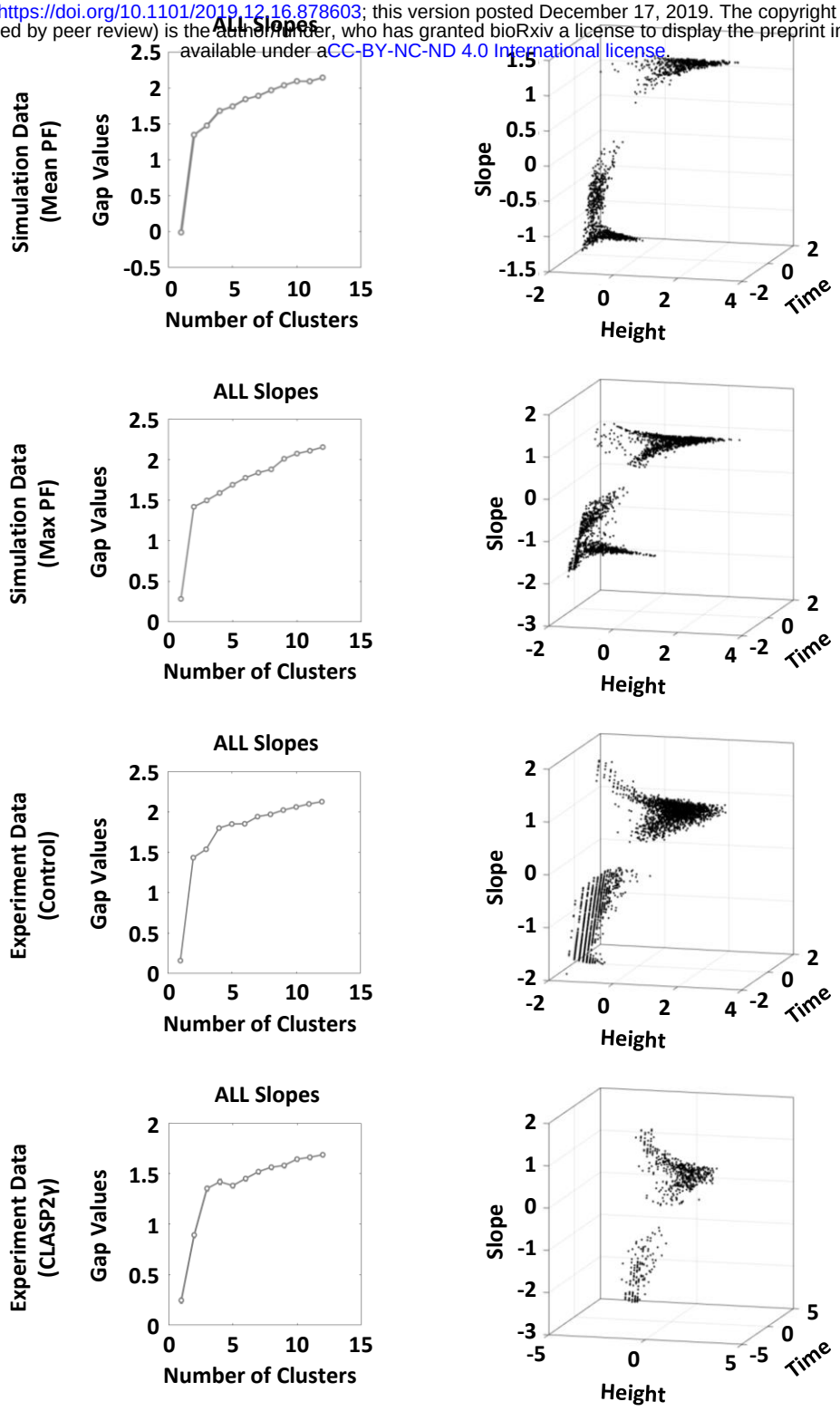

Figure S6. Gap Statistic plots and segment feature plots for an analysis where all slope segments in each data set were considered together (excluding flat segments), not separated into positive and negative slopes as in Figures S4 and S5. Note that the gap statistic plots are monotonically increasing, indicating that the initial dataset was too complex for effective identification of an optimal *k*-value for clustering (for this reason, the data are not color-coded as in the previous two figures). If the two-state model were correct, one might expect that the dataset would be optimally separable into two groups, and that the gap statistic plot would attain its first local maximum at *k*=2. However, even when the two-state conclusion is assisted by removing segments with slope or length change approximately equal to zero, providing a clear band of separation between growth and shortening (as is depicted in this figure), *k*=2 is still not suggested by the gap statistic. This result indicated that we needed to subdivide the dataset before further analysis (Tibshirani, Walther, and Hastie 2001). Combined with established knowledge of mechanistic differences between growth and shortening, we chose to treat positive and negative separately.

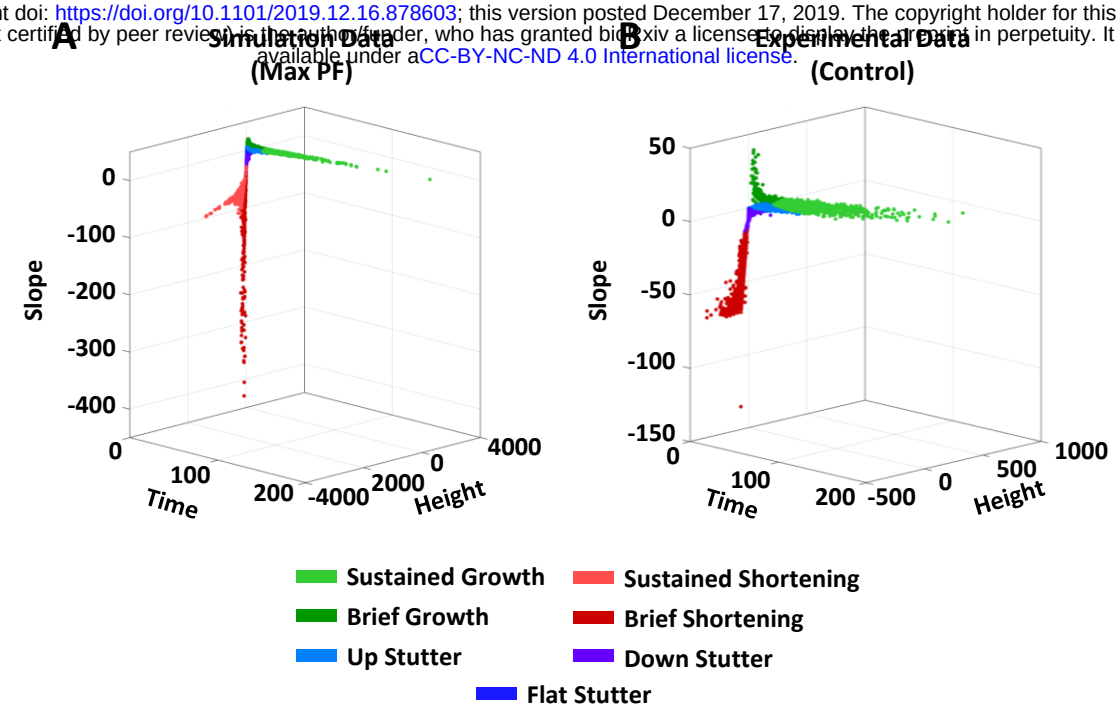

Figure S7. Clustering profiles for ALL segments of *in silico* and *in vitro* data. Following separate classification of the positive and negative slopes (see Figures S4 and S5), segment data is un-log-transformed and unstandardized for full view of line segment data in 3-D space. Note that the classification step has already taken place, and these figures are simply for visualizing how the clusters exist in relation to each other in 3-D space.

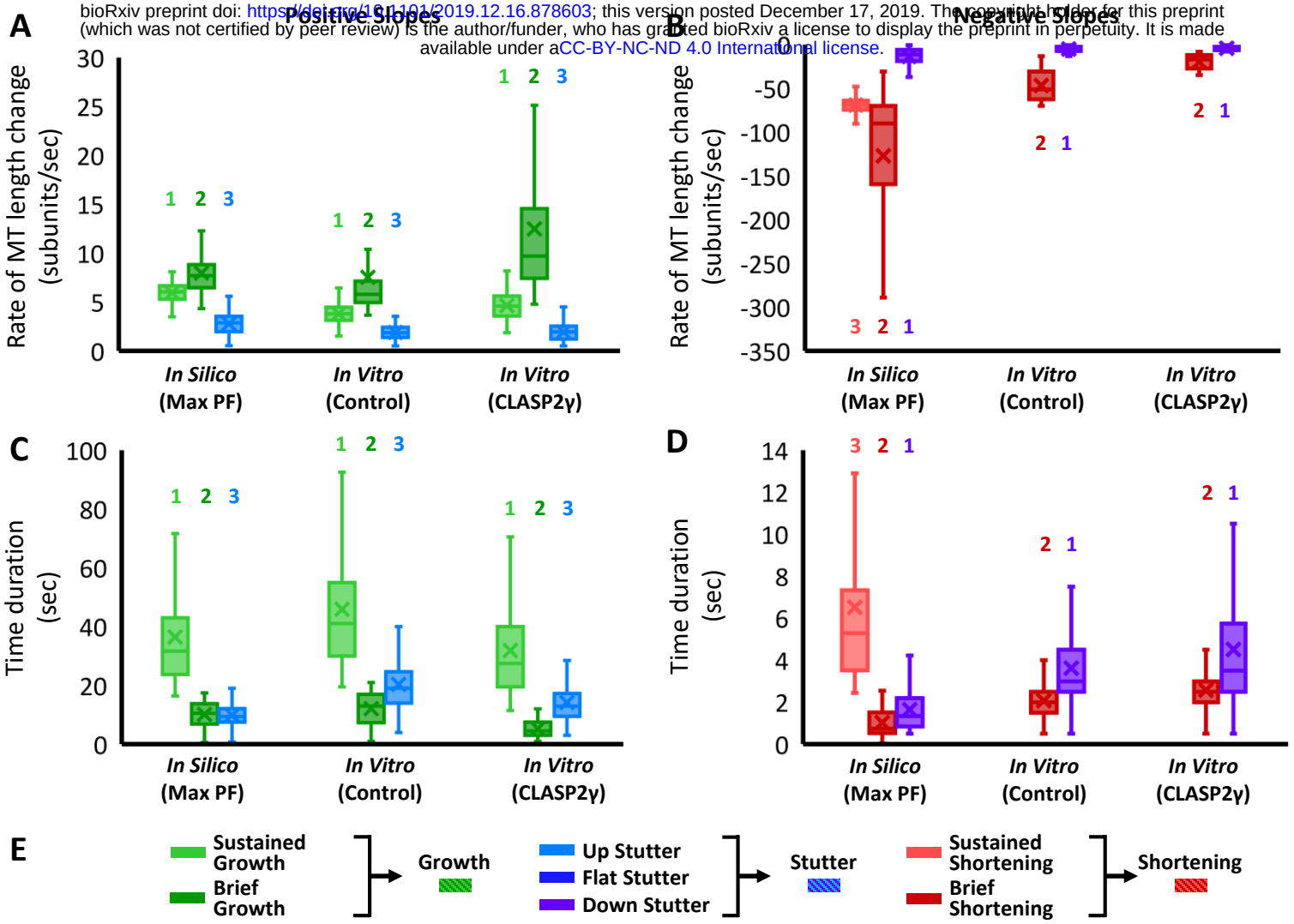

Figure S8. Box and whisker plots of rates of MT length change (subunits/sec) and time durations for different subgroups across data sets to motivate subsequent bundling (box and whiskers cover the four quartiles of each subset, and the 'X' marks the mean value in the plots). *Note: the first two data sets in A and B are the same as the data presented in Figure 3 C and F, respectively*. **(A)** Growth rates for the positive sloped segment clusters identified in the simulation data sets and the experimental data sets without and with CLASP2γ. In each data set, two clusters (light and dark green) had average growth rates relatively large in magnitude compared to the third (light blue). **(B)** Shortening rates for the negative sloped segment clusters identified in the simulation data and in the experimental data sets without and with CLASP2γ. In each data set, the red-labeled shortening rates were on average relatively large in magnitude compared to the purple-labeled group. **(C)** Time durations for the positive sloped segment clusters show that one subset of segments (light green) represents a longer, more sustained period of consistent behavior than the other two subsets (blue and dark green) for all data sets considered. **(D)** Time durations for negative sloped segment clusters from simulation data also shows that one subset (light red) represents a longer, more sustained period of consistent behavior than the other two subsets (purple and dark red). Since the experimental data did not capture most of the shortening behavior, analysis of longer time duration shortening segments was not possible for the *in vitro* data sets. **(E)** Bundling subgroups together into larger phase classes based on the average slopes of individual clusters. Clusters with positive and negative slopes relatively larger in magnitude were bundled together into 'Growth' and 'Shortening' phases respectively. The remaining clusters, where significantly less changes in length occur, were bundled together, along with the previously identified 'near zero' slope or flat segments, into a new phase called 'Stutters'. Further, 'Brief' and 'Sustained' sub-classes of the Growth and Shortening phases were characterized by their time durations. The 'Up', 'Flat', and 'Down' sub-classes of the Stutter phase are characterized by the segment slope being positive, near-zero, or negative respectively.

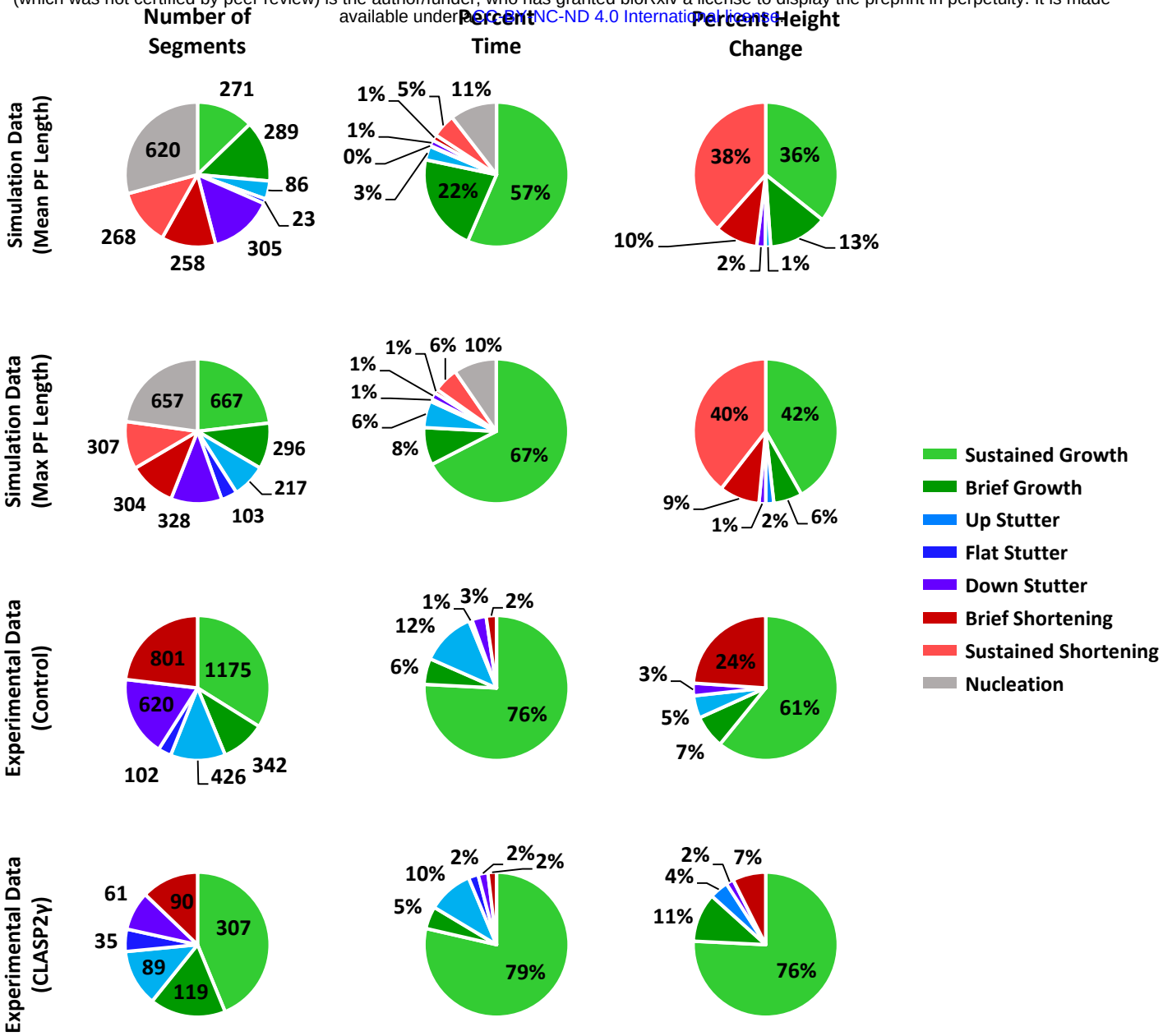

Figure S9. Segment statistics for all *in silico* and *in vitro* data sets. *Number of segments*, *percent time*, and *percent height change* for each cluster are recorded for each data set. For the *in silico* data sets where depolymerizations were fully captured, the breakdown of the number of segments, time duration, and height change are representative of the actual time the simulated MT spent in the various phases. As noted throughout the paper, the *in vitro* depolymerizations were not captured in their entirety, and so the number of negative slope segments, percent time, and the percent height change attributed to negatively sloped MT behavior is largely underreported.

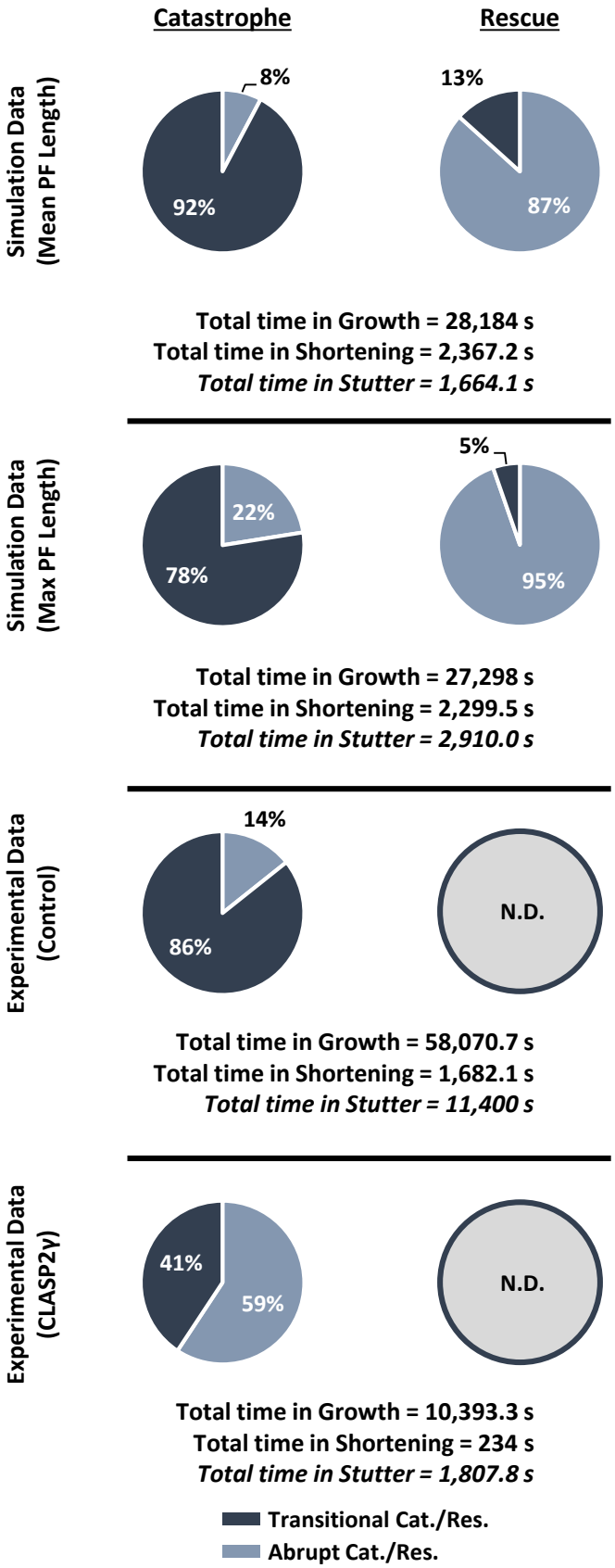

Transition Statistics		
	Count	**Frequency (s^{-1})**
Simulation Data (Mean PF Length)		
Abrupt Catastrophe	20	0.00071
Transitional Catastrophe	238	0.0084
Total Catastrophe	**258**	**0.00911**
Abrupt Rescue	39	0.0164
Transitional Rescue	6	0.0025
Total Rescue	**45**	**0.0189**
Interrupted Growth	75	0.0027
Interrupted Shortening	32	0.0135
Simulation Data (Max PF Length)		
Abrupt Catastrophe	67	0.0025
Transitional Catastrophe	231	0.0085
Total Catastrophe	**298**	**0.0110**
Abrupt Rescue	71	0.0307
Transitional Rescue	4	0.0017
Total Rescue	**75**	**0.0324**
Interrupted Growth	293	0.0107
Interrupted Shortening	48	0.0207
Experimental Data (Control)		
Abrupt Catastrophe	105	0.0018
Transitional Catastrophe	629	0.0108
Total Catastrophe	**734**	**0.0126**
Abrupt Rescue	**N.D.**	
Transitional Rescue		
Total Rescue		
Interrupted Growth	211	0.0036
Interrupted Shortening	0	0
Experimental Data (CLASP2γ)		
Abrupt Catastrophe	51	0.0049
Transitional Catastrophe	35	0.0034
Total Catastrophe	**86**	**0.0083**
Abrupt Rescue	**N.D.**	
Transitional Rescue		
Total Rescue		
Interrupted Growth	92	0.0088
Interrupted Shortening	1	0.0043

Figure S10. Detailed transition statistics for each data set. Both *in silico* data sets as well as the control experimental data set demonstrate that a significant majority of catastrophes occur via stutter (i.e., transitional catastrophe), while the CLASP2γ data set shows a shift to MTs exhibiting abrupt catastrophes. We speculate that the shift to abrupt catastrophes is due to CLASP2γ promoting tip extensions (see the Results and Discussion for more information on mechanistic speculation regarding the effects of CLASP2γ). Rescue data for *in silico* MTs indicates clearly that rescues largely occur abruptly. Note that rescue metrics were not determined (N.D.) for the *in vitro* data due to a lack of depolymerizations captured for *in vitro* MTs.

STADIA: User-defined Parameters	
Nucleation height threshold	75 subunits
Minimum time duration of a linear segment	500 ms
Maximum height error tolerance	20 subunits
Maximum height change for near-zero slope segments	3 subunits
Maximum slope magnitude for near-zero slope segments	0.5 subunits/sec
Number of centroids for positive slope segments	3
Number of centroids for negative slope segments (*in silico* data)	3
Number of centroids for negative slope segments (*in vitro* data)	2

Classical Analysis: User-defined Parameters	
Minimum peak height	95 subunits
Minimum rescue length	95 subunits
Minimum Prominence For Major Peaks	20 subunits
Minimum Prominence For Minor Peaks	0.1 subunits
Minimum Regression R^2	0.95

Table S1. User-defined parameters for STADIA and classical analysis.

13-PF Detailed MT Computational Model Parameters	
Number of protofilaments	13
Tubulin concentration	10 μM
Simulation time	10 hours
Seam shift	1.5 subunit lengths
Compete for tubulin	No
Hydrolysis rate	0.7 subunits/sec
HalfMax	200
kgrowT	250
kgrowD	250
kshortT	0.02
kshortD	20
kbondTT	100
kbondTD	100
kbondDT	100
kbondDD	100
kbreakTT	70
kbreakTD	90
kbreakDT	90
kbreakDD	400
SkbondTT	200
SkbondTD	200
SkbondDT	200
SkbondDD	200
SkbreakTT	140
SkbreakTD	180
SkbreakDT	180
SkbreakDD	800

Table S2. Computational model parameters used to generate simulation data. Parameters used are from Margolin et al. 2012.

SUPPLEMENTAL MATERIAL

DATA ACQUISITION: *IN SILICO* MICROTUBULE EXPERIMENTS

This section outlines the details regarding the acquisition of simulation MT data including information about both the model and the parameters used.

The computational model: Stochastic model for simulating 13-protofilament (13-PF) MTs

The computational MT model used in this paper to generate the *in silico* length-history data was an updated version of the detailed, stochastic MT model published in (Margolin et al. 2012), which is a kinetic Monte Carlo simulation that tracks the state of individual subunits (representing tubulin dimers) in the entire 13-protofilament MT structure. Simulation of MTs is done using biochemical rate constants in conjunction with the Gillespie algorithm (Gillespie 1976, 1977) to sample event times and to build a stochastic simulation of individual molecular-level events (e.g., formation/breaking of longitudinal and lateral bonds, and hydrolysis). A key difference between the previous versions and the current computational model is strict adherence to the assumption that only one of the many possible biochemical events occurs at a time. The previous detailed level 13-PF MT model approximated hydrolysis events by allowing several subunits to hydrolyze simultaneously after one of the other four reaction events (lateral bonding/breaking or subunit gain/loss) have occurred. Hydrolysis events are now considered as a possible event in the same way that the others are handled. This modification resulted in very little change in macro-level behavior of *in silico* MTs, but the ability to output dedicated observations to each dimer-level event is a more accurate representation of MT biochemistry. The overall result of the simulation is *in silico* MTs that exhibit macro-level DI behaviors in agreement with those observed for previously (Margolin et al. 2012).

Simulation setup and parameters

The dimer-scale kinetic parameters used in this study to simulate a 13-protofilament MT using the model described above were tuned in (Margolin et al. 2012) based on *in vitro* DI measurements from (Walker et al. 1988); a detailed list of parameters can be found in **SuppMat Table S2**. For the purposes of this analysis, a single non-competing MT was simulated at a constant [free tubulin] of 10 µM for 10 hours of simulation time. The max PF length (i.e., the length of the longest of the 13 protofilaments) was reported as the length of the MT, which was used to generate a length-history plot passed into STADIA. Though the mean PF length could have been used to represent the length of the entire MT, better agreement with the *in vitro* data used here was found using the max PF length instead (see clustering profiles in **SuppMat Figure S4**).

DATA ACQUISITION: *IN VITRO* MICROTUBULE EXPERIMENTS

This section outlines the details regarding capture of experimental MT data including conditions for a control group (tubulin + EB1) and a group with MTBPs (tubulin + EB1 + CLASP2γ). A subset of the *in vitro* dataset was previously published in (Lawrence et al. 2018).

Protein preparation

His-CLASP2γ and His-EB1 were purified as previously described (Zanic et al. 2013; Lawrence et al. 2018). Bovine brain tubulin was purified using the high-molarity method (Castoldi and Popov 2003). Tubulin

was labeled with TAMRA and Alexa Fluor 488 (Invitrogen) according to the standard protocols, as previously described (Hyman et al. 1991).

TIRF microscopy

Imaging was performed using a Nikon Eclipse Ti microscope with a 100×/1.49 n.a. TIRF objective, NEO sCMOS (complementary metal–oxide–semiconductor) camera; 488- and 561- solid-state lasers (Nikon Lu-NA); Finger Lakes Instruments HS-625 high speed emission filter wheel; and standard filter sets. An objective heater was used to maintain the sample at 35°C. Microscope chambers were constructed as previously described (Gell et al. 2010). In brief, 22 × 22 mm and 18 × 18 mm silanized coverslips were separated by strips of Parafilm to create a narrow channel for the exchange of solution (Gell et al. 2010). Images were acquired using NIS-Elements (Nikon).

Dynamic MT Assay

GMPCPP-stabilized MTs were prepared according to standard protocols (Hyman et al. 1992; Gell et al. 2010). Dynamic MT extensions were polymerized from surface-immobilized GMPCPP-stabilized templates as described previously (Gell et al. 2010). The imaging buffer consisted of BRB80 supplemented with 40 mM glucose, 40 µg/ml glucose oxidase, 16 µg/ml catalase, 0.5 mg/ml casein, 100 mM KCl, 10 mM DTT, and 0.1% methylcellulose. The imaging buffer containing 1 mM GTP and purified proteins was introduced into the imaging chamber. Dynamic MTs were grown with 12 µM Alexa 488-labeled tubulin and 200 nM EB1 with or without 400 nM CLASP2γ and imaged at 2 fps using a 100× objective and an Andor Neo camera (pixel size of 70 nm). Alexa-488-labeled tubulin was used at ratio of 23% of the total tubulin. Dynamic MT tip positions as a function of time were determined by kymograph analysis using KymographDirect and KymographClear (Mangeol, Prevo, and Peterman 2016).

***In vitro* MT length-history data**

Length-history data for *in vitro* MTs was obtained from 30 minute-long experiments using both a control group and a group with the stabilizing MTBP, CLASP2γ. The control group data was acquired from 68 MT seeds, from which 776 individual traces were observed. The group with CLASP2γ was acquired from 29 MT seeds, from which 85 individual traces were observed. After applying the stitching preprocessing step during the STADIA segmentation stage, the control group and the group with CLASP2γ each generated a single stream time series representing length-history data with total time duration over 21 hours and 3.5 hours respectively. The collective consideration of all experimental data samples together meets the needs of the machine learning requirements for reliable clustering results (i.e., the lifetime of a single MT alone would not be a sufficient amount of data for *k*-means clustering).

REFERENCES

Castoldi, Mirco, and Andrei V. Popov. 2003. "Purification of Brain Tubulin through Two Cycles of Polymerization–Depolymerization in a High-Molarity Buffer." *Protein Expression and Purification* 32 (1): 83–88. https://doi.org/10.1016/S1046-5928(03)00218-3.

Gell, Christopher, Volker Bormuth, Gary J. Brouhard, Daniel N. Cohen, Stefan Diez, Claire T. Friel, Jonne Helenius, et al. 2010. "Microtubule Dynamics Reconstituted in Vitro and Imaged by Single-Molecule Fluorescence Microscopy." *Methods in Cell Biology* 95 (January): 221–45. https://doi.org/10.1016/S0091-679X(10)95013-9.

Gillespie, Daniel T. 1977. "Exact Stochastic Simulation of Coupled Chemical Reactions." *Journal of Physical Chemistry* 81 (25): 2340–61. https://doi.org/10.1021/j100540a008.

Gillespie, Daniel T. 1976. "A General Method for Numerically Simulating the Stochastic Time Evolution of Coupled Chemical Reactions." *Journal of Computational Physics* 22 (4): 403–34. https://doi.org/10.1016/0021-9991(76)90041-3.

Hyman, A. A., S. Salser, D. N. Drechsel, N. Unwin, and T. J. Mitchison. 1992. "Role of GTP Hydrolysis in Microtubule Dynamics: Information from a Slowly Hydrolyzable Analogue, GMPCPP." *Molecular Biology of the Cell* 3 (10): 1155–67. https://doi.org/10.1091/mbc.3.10.1155.

Hyman, Anthony, David Drechsel, Doug Kellogg, Steve Salser, Ken Sawin, Pam Steffen, Linda Wordeman, and Tim Mitchison. 1991. "Preparation of Modified Tubulins." *Methods in Enzymology* 196 (January): 478–85. https://doi.org/10.1016/0076-6879(91)96041-O.

Lawrence, Elizabeth J., Göker Arpag, Stephen R. Norris, and Marija Zanic. 2018. "Human CLASP2 Specifically Regulates Microtubule Catastrophe and Rescue." *Molecular Biology of the Cell* 29 (10): 1168–77. https://doi.org/10.1091/mbc.E18-01-0016.

Mangeol, Pierre, Bram Prevo, and Erwin J.G. Peterman. 2016. "KymographClear and KymographDirect: Two Tools for the Automated Quantitative Analysis of Molecular and Cellular Dynamics Using Kymographs." *Molecular Biology of the Cell* 27 (12): 1948–57. https://doi.org/10.1091/mbc.E15-06-0404.

Margolin, Gennady, Ivan V Gregoretti, Trevor M Cickovski, Chunlei Li, Wei Shi, Mark S Alber, and Holly V Goodson. 2012. "The Mechanisms of Microtubule Catastrophe and Rescue: Implications from Analysis of a Dimer-Scale Computational Model." *Molecular Biology of the Cell* 23 (4): 642–56. https://doi.org/10.1091/mbc.E11-08-0688.

Walker, R. A., E. T. O'Brien, N. K. Pryer, M. F. Soboeiro, W. A. Voter, H. P. Erickson, and E. D. Salmon. 1988. "Dynamic Instability of Individual Microtubules Analyzed by Video Light Microscopy: Rate Constants and Transition Frequencies." *The Journal of Cell Biology* 107 (4): 1437–48. https://doi.org/10.1083/jcb.107.4.1437.

Zanic, Marija, Per O. Widlund, Anthony A. Hyman, and Jonathon Howard. 2013. "Synergy between XMAP215 and EB1 Increases Microtubule Growth Rates to Physiological Levels." *Nature Cell Biology* 15 (6): 688–93. https://doi.org/10.1038/ncb2744.